

BOSTON UNIVERSITY
COLLEGE OF ENGINEERING

Thesis

**DEVELOPMENT OF A FLEXIBLE MODELING
ENVIRONMENT FOR EVALUATING SUBCORTICAL
AUDITORY SYSTEMS**

by

GRAHAM VOYSEY

B.S., Boston University, 2006

Submitted in partial fulfillment of the
requirements for the degree of
Master of Science

2016

© 2016 by
GRAHAM VOYSEY
CC BY

Approved by

First Reader

H. Steven Colburn, PhD
Professor of Biomedical Engineering

Second Reader

Barbara Shinn-Cunningham, PhD
Professor of Biomedical Engineering

Third Reader

Allyn E. Hubbard, PhD
Professor of Electrical and Computer Engineering
Professor of Biomedical Engineering

Fourth Reader

Hideko Nakajima, MD, PhD
Assistant Professor of Otology and Laryngology
Harvard Medical School, Massachusetts Eye and Ear Infirmary

We've heard a lot of models... and heard suggested that we should take things out of our models to figure out what's important. But in some sense, when I look at the diversity of models that have been presented so far—each of us leave *out* things. So maybe in some sense we've got a start towards that approach.

So I can ask this question two ways, but let me ask it this way: *What should we leave in?* What's the bare minimum we should leave in as we try to understand what's important about the function of the cochlea?

*David C. Mountain
Mechanics of Hearing (Attica, Greece 2014)*

Acknowledgments

I begin by thanking my advisor in so many things, Dr. H. Steven Colburn, who has been an aspirational example to me for more than a decade. Thank you for your support and care. Thank you for helping me find the questions I want to answer.

I'd also like to thank my committee members, Dr. Barbara Shinn-Cunningham, Dr. Allyn Hubbard, and Dr. Hideko Nakajima. Barb, thank you for being the example by which I judge the clarity of talks, and for introducing me to the complexities of the auditory system. Al and Heidi, thank you for your careful attention and engaging discussions.

I would not have been able to complete this work without the help of many of my colleagues and fellow researchers. I am deeply indebted first to Dr. Goldbarg Mehraei, for graciously sharing her experimental data and knowledge with me. My sincere gratitude to Dr. Sarah Verhulst and her group for sharing their model code with me, and Dr. Laurel Carney for a series of formative conversations that shaped how this project proceeded. I'd also like to thank Gerard Encina-Llamas for being the first user of the software I developed during the course of this thesis, and for suggesting many valuable additions I wouldn't have thought of alone.

I'd like to thank all my colleagues in the Hearing Research Center. In particular, Aleks Zosuls and Andy Brughera have been good friends and valuable resources for many years, and I'm very grateful. I'd especially like to thank my friend Dave Anderson, whose mentorship is the direct cause of my skills in software development and project architecture design, without which this or any other computational project would've been impossible.

I would like to thank many people in my private life for their support and encourage-

ment: My wife, Yelena, for her tireless support, unconditional love, and tolerance of late nights in the lab, and my son Rory, who may be too young to know how helpful he's been in motivating me. My brother, Ian, for living out the Voysey byword, and my parents, Helen and Stephen, for instilling in me the tenacity to stay with the work, and the desire to do things that make a difference.

Finally, I'd like to thank David Mountain, who saw something worthy in me. Thank you for setting the bar so high, and showing me what a life spent in an exuberant search for answers looks like.

DEVELOPMENT OF A FLEXIBLE MODELING ENVIRONMENT FOR EVALUATING SUBCORTICAL AUDITORY SYSTEMS

GRAHAM VOYSEY

ABSTRACT

Cochlear Synaptopathy (CS) is an emerging topic of hearing research that focuses on peripheral pathologies which leave audiometric thresholds unchanged but significantly impair threshold-independent hearing performance. Primary among the proposed mechanisms of CS is selective damage of low spontaneous rate (low SR) fibers of the auditory nerve (AN), yet no noninvasive quantitative measure of CS yet exists in humans.

This work aimed to explore the hypothesis that measuring changes in latency of Wave V of the Auditory Brainstem Response (ABR) can predict the magnitude of preferentially damaged contributions by low spontaneous rate fibers to the output of the auditory nerve. While steps towards establishing a relationship between Wave V latencies and a psychophysical measure of CS has been recently undertaken in human experiments (Mehraei et al., 2016), current biophysical models do not fully account for the observed results.

To begin to address the discrepancies between these experiments and biophysical models of hearing, a new comprehensive modeling tool was developed which allows parametric exploration of modeling space and direct comparison between major models of the auditory nerve and brainstem.

It is hypothesized that modeling deficits may be in part a consequence of the defi-

iciencies of current brainstem and midbrain models, including those of the Inferior Colliculus (IC) and Lateral Lemniscus (LL), where Wave V is thought to originate. To rectify those deficiencies, more sophisticated models of the midbrain and brainstem were incorporated into the new modeling tool. Incorporating recent anatomical and electrophysiological results, which suggest a varying contribution of low-SR fibers for different audible frequencies, further addresses modeling efficacy.

Contents

1	Introduction	1
1.1	Motivation	1
1.2	Implication of the Auditory Periphery in Cochlear Synaptopathy	1
1.3	Human Psychophysical Tests Suggest a Diagnostic Measure	2
1.4	Computational Models of the Periphery are not Predictive	3
1.5	An Improved Modeling Approach	4
2	Literature Review	5
2.1	Chapter Summary	5
2.2	Cochlear Synaptopathy	5
2.3	Physiology of the Auditory Nerve	7
2.3.1	Spontaneous Rates of Fibers	7
2.3.2	Low Spontaneous Rate Fibers Suffer Selective Losses	7
2.3.3	Fiber SR Distribution is Not Tonotopically Uniform	8
2.4	Relevant Functional Neuroanatomy of the Auditory Midbrain	9
2.4.1	The Cochlear Nucleus	10
2.4.2	The Dorsal Cochlear Nucleus	11
2.4.3	The Inferior Colliculus	11
2.5	Models of the Auditory Periphery	13
2.5.1	The Verhulst Model	13
2.5.2	The Zilany and Bruce Model	13
2.6	Models of the Auditory Midbrain and Brainstem	16

2.6.1	The Nelson-Carney Model	16
2.6.2	The Carney Model	16
2.7	The Auditory Brainstem Response	20
2.8	Candidate Objective Measures of Cochlear Synaptopathy in Humans	21
3	Aims	23
3.1	Aim I. Simulate the ABR Response of a Noise-Masking Task with Variable SR Contributions and Model Parameters	23
3.2	Aim II. Integrate Improved Brainstem Models	24
3.3	Aim III. Relate Model Responses to Psychophysical Measures	25
4	The Corti Modeling Framework	26
4.1	Chapter Summary	26
4.2	Overview of Modeling Framework	26
4.2.1	Software Design	27
4.2.2	Configuration Options Define a Parameter Space	28
4.3	Simulation using Corti	28
4.4	Peripheral Models	30
4.4.1	The Verhulst Model	30
4.4.2	The Zilany Model	32
4.4.3	Accounting for Variations in Spontaneous Rates Between Models	32
4.4.4	Peripheral Model Output	33
4.5	Auditory Nerve Response Models	34
4.5.1	Modeling the Contributions of Inner Hair Cells	34
4.5.2	Weighting of IHC contributions	36
4.5.3	Weighting of Fiber Types per IHC	36
4.5.4	Modeling Synaptopathy	39
4.6	Brainstem Models	40

4.6.1	Choice of Best Modulation Frequency	40
4.6.2	The Nelson Carney 2004 Brainstem	41
4.6.3	The Carney 2015 Brainstem	42
4.7	Stimulus Generation	43
4.8	Automated Parameter Exploration	43
4.8.1	Design of New Experiments	44
5	Results	45
5.1	Chapter Summary	45
5.2	Modeling a Human Noise-Masked ABR	45
5.3	Quantification of Model Changes are Level Sets	45
5.3.1	Stimuli	46
5.4	Effect of Cochlear Synaptopathy	46
5.5	Effect of Peripheral Model Choice	49
5.6	Effect of CF weighting	51
5.7	Effect of Brainstem Model Choice	51
6	Discussion	54
6.1	Chapter Summary	54
6.2	Nonlinear Behaviors in the Verhulst Model	54
6.3	Consequences of AN Population Response Modeling	55
6.4	Nonlinear Synaptopathic Models	56
7	Conclusion	58
7.1	Summary	58
7.2	Future Directions	59
7.2.1	Modeling of Specific Hearing Loss Types	59
7.2.2	Anatomically Inspired IC Weighting	60

List of Figures

2.1	Deafferentiation of Inner Hair Cells	6
2.2	Synaptopathy is Selective	8
2.3	Distribution of Fiber Type	9
2.4	Ascending Auditory Pathway	10
2.5	Low SR Fibers Project to the Small Cap	12
2.6	The Verhulst Model	14
2.7	The Zilany Model	15
2.8	The Nelson and Carney Model	17
2.9	The Carney 2015 Model	18
2.10	IC Response Types	19
2.11	The Auditory Brainstem Response	20
2.12	Wave V latency in noise	22
4.1	Overview of the Corti Modeling Environment.	29
4.2	The Peripheral Stage	31
4.3	The Auditory Nerve Stage	35
4.4	Variation in Spontaneous Rate as a Function of Frequency	37
4.5	Cochlear Synaptopathy Parameters	39
4.6	The Brainstem and Midbrain Stage	40
4.7	Overview of the Nelson-Carney Midbrain and Brainstem	41
4.8	Overview of the Carney Midbrain and Brainstem	42
4.9	Automated Exploration of Model Parameters	44

5.1	Experimental Stimuli	47
5.2	Effects of Synaptopathy	48
5.3	Effects of Peripheral Models	50
5.4	Effects of CF Weighting	52
5.5	Effects of Brainstem Models	53

List of Abbreviations

ABR	Auditory Brainstem Response
AN	Auditory Nerve
ANR	Auditory Nerve Response
CAP	Compound Action Potential
CN	Cochlear Nucleus
CS	Cochlear Synaptopathy
DPOAE	Distortion Product Otoacoustic Emission
HDF5	Hierarchical Data Format Version Five
HHL	Hidden Hearing Loss
IC	Inferior Colliculus
IFR	Instantaneous Firing Rate
NIHL	Noise Induced Hearing Loss
OAE	Otoacoustic Emission
PTA	Pure Tone Audiometry
PTS	Permanent Threshold Shift
SR	Spontaneous Rate
TTS	Temporary Threshold Shift

Chapter 1

Introduction

1.1 Motivation

The variability of overall performance between putatively normal hearing listeners, particularly in supra-threshold tasks performed in complex acoustic environments such as the cocktail party problem, has been recognized in the literature for many years (Cherry, 1953). Until recently, this variability was largely attributed to a broadly-defined “Central Processing Disorder” in the absence of clinical Noise-Induced Hearing Loss (NIHL). The performance of the auditory periphery has been thought to be sufficiently characterized by pure tone audiometry (PTA), as well as Distortion-Product Otoacoustic Emissions (DPOAEs) and Auditory Brainstem Responses (ABR) for more detailed assessment of individual areas of the peripheral auditory system.

1.2 Implication of the Auditory Periphery in Cochlear Synaptopathy

Recently, selective deafferentiation of low spontaneous rate (low SR) fibers of the AN in the auditory periphery that do not affect audiometric thresholds have been convincingly demonstrated in mouse (Kujawa & Liberman, 2009), gerbil (Furman, Kujawa, & Liberman, 2013), and recently, chinchilla (Liberman, unpublished); a

growing body of psychophysical evidence suggests that a similar pathology occurs in humans (Bharadwaj, Masud, Mehraei, Verhulst, & Shinn-Cunningham, 2015). In mice, synaptic damage at the hair cell in the Organ of Corti has been observed both in response to noise with intensities sufficient to induce a temporary threshold shift (TTS), which does not permanently affect Compound Action Potential (CAP) thresholds or hair cell viability, and due to age alone in quiet (Sergeyenko, Lall, Liberman, & Kujawa, 2013; Fernandez, Jeffers, Lall, Liberman, & Kujawa, 2015). This phenomenon has been variously described as “cochlear synaptopathy” (CS) (Bharadwaj, Verhulst, Shaheen, Liberman, & Shinn-Cunningham, 2014), “auditory neuropathy”, or “Hidden Hearing Loss” (HHL).

It is now thought that selective low-SR loss may be a hallmark of HHL (Furman et al., 2013; Bharadwaj et al., 2014; Bharadwaj et al., 2015; Schaette & McAlpine, 2011). Consequently, it has been implicated in performance degradation in cocktail party scenarios in normal-hearing listeners (Bharadwaj et al., 2015; Bharadwaj et al., 2014). Unlike NIHL, no objective and noninvasive measure of HHL in humans has been established. While work is ongoing in cadaveric studies, the relationship between low-SR damage and HHL in humans has relied on inference from a combination of ABR, DPOAE, and psychometric measures, and no direct measure has yet been demonstrated that specifically implicates low-SR fiber loss as a sufficient causative factor for HHL.

1.3 Human Psychophysical Tests Suggest a Diagnostic Measure

Towards this goal of defining an objective measure of fiber loss, Mehraei, Gallardo, Epp, Shinn-Cunningham, and Dau, 2015; Mehraei et al., 2016 have performed a series

of experiments that relate psychophysical performance in a tone-in-notched-noise ITD detection task to measured latency changes in ABR Wave V as a function of signal to noise ratio. They hypothesized that the loss of low-SR/high-threshold AN fibers would contribute to a faster recovery time of the compound action potential of the AN. In a perceptual task, this translates to higher thresholds, and faster threshold recovery. In a group of 28 normal hearing threshold (NHT) subjects, comparison of ABR data and psychoacoustic performance demonstrate a relationship consistent with an impairment in low-SR population response (Mehraei et al., 2016).

1.4 Computational Models of the Periphery are not Predictive

While psychophysical experiments have supported the hypothesis of the importance of low-SR fibers, modeling the response of the auditory periphery, brainstem, and midbrain to the stimuli used in experiments has so far failed to produce results that are with experimental results (Mehraei et al., 2016).

Many disparate models of different stages of the subcortical auditory system have been developed and are in common use. Among these are models of the middle ear, the auditory nerve, and the auditory processing areas of the brainstem and the midbrain. Any given computational model of a particular area may be optimized by its authors for particular objectives that may not be shared by other models of the same area; further, the inputs required for more than one model of a given area may be dissimilar, and the outputs may also vary considerably. Numerous projects exist to address some of these difficulties. Among these projects are EarLab (<http://earlab.bu.edu>), the Auditory Modeling Toolbox (<http://amtoolbox.sourceforge.net>), and the Cochlea modeling environment (<https://github.com/mrkrd/cochlea>) (Rudnicki & Hemmert,

2014).

To date, no project fully addresses the modeling concerns that arise during the study of the role of the precortical auditory system in HHL. Further, no project currently addresses the need to easily compare the performance and behavior of individual models as they are used to study the same problems.

1.5 An Improved Modeling Approach

This work sought to extend the modeling of the peripheral and central auditory system performed by Mehraei, 2015 by creating a modeling framework that allows the direct comparison of the relative effects of leading acoustic models, with two novel modeling features also incorporated.

A framework for the design of arbitrarily complex future modeling experiments that automatically incorporates permutations of model choice and model parameters was also developed to provide a modeling comparison tool to the research community.

Chapter 2

Literature Review

2.1 Chapter Summary

This chapter lays out a review of the relevant literature this thesis relies on. First, an overview of the clinical significance and relevant neuroanatomy of cochlear synaptopathy are given. Then, a review of the computational models that will be used for the body of this thesis is presented.

2.2 Cochlear Synaptopathy

Deafferentiation is the loss of one or more afferent synapses between an Inner Hair Cell (IHC) and its innervating spiral ganglia. As a result of this synaptopathy, fewer channels are available to transmit information from the IHC through the AN to the brain, and the fidelity of the signal is degraded.

Kujawa and Liberman, 2009 showed in noise exposed mice that significant deafferentation can occur with no permanent changes in threshold tuning curves and no hair cell death. Figure 2.1 shows that deafferentation was confirmed histologically by triple-staining cross-sections of the Organ of Corti post noise exposure. This reveals a synaptic loss.

Sergeyenko et al., 2013 extended this work to demonstrate that this deafferentiation

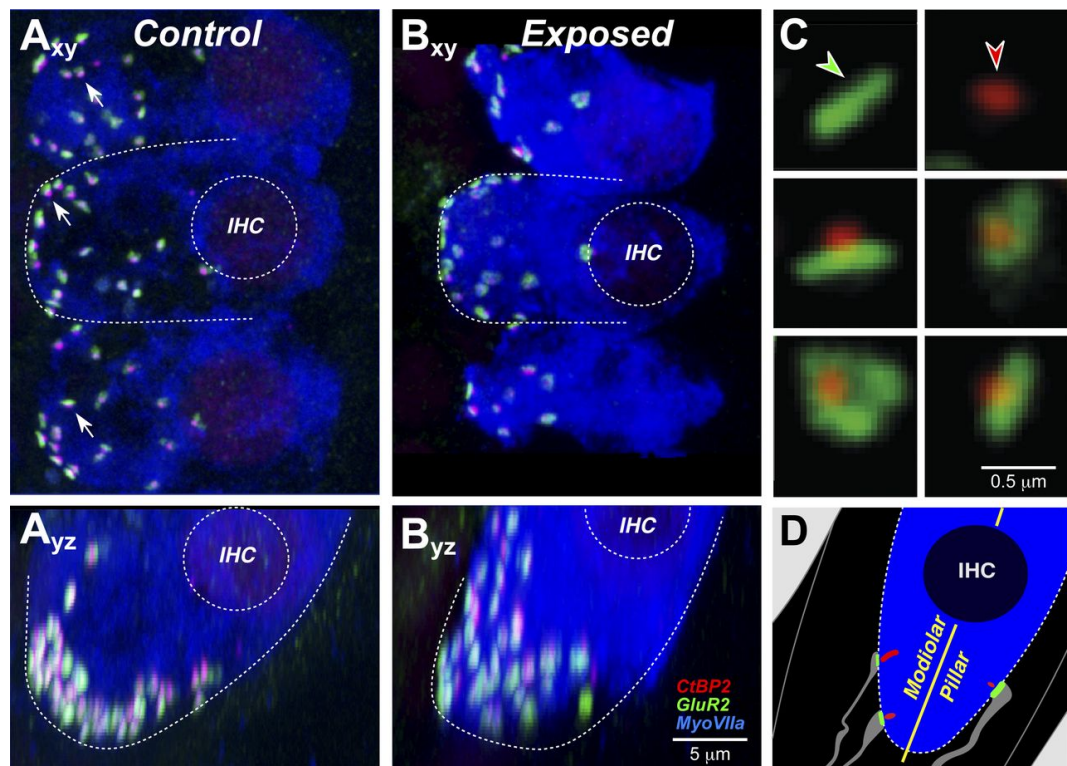


Figure 2.1: Deafferentiation of IHCs precedes hair cell death in noise exposed mice. Figure is reprinted from Furman, Kujawa, and Liberman, 2013. Panels A and B show a triple-stained cross sectional view of an IHC. Synaptic ribbons are in red, and glutamate-receptor patches are in green; deafferentiation is visible when they are not paired (in C).

may also arise solely as a function of time. In a study of mice aged 4 to 144 weeks that were never exposed to loud sounds, a similar loss of hair cell projections was observed.

2.3 Physiology of the Auditory Nerve

The auditory nerve is comprised of tens of thousands of auditory nerve fibers. Each fiber synapses on a particular IHC, and encodes information about the deflection of the IHC bundle as a result of motion of the basilar membrane that, in turn, was evoked by a sound pressure wave.

2.3.1 Spontaneous Rates of Fibers

In the absence of stimulus, individual fibers of the auditory nerve exhibit a wide range of average firing rates: human AN fibers have spontaneous rates between 0–120 spikes/second. Any individual fiber's spontaneous rate varies slowly over time, but will fall within a relatively narrow band. The fibers of the auditory nerve are divided into two, or sometimes three, categories: low-, medium-, and high spontaneous rate (SR). Different authors assign different maximum firing rates to each category: Temchin, Rich, and Ruggero, 2008 categorizes SRs below 18 spikes/second to be “low/medium”, and anything above that to be “high”. Others, such as Liberman, 1978, define only two categories.

2.3.2 Low Spontaneous Rate Fibers Suffer Selective Losses

Furman et al., 2013 and others have demonstrated that noise-induced cochlear synaptopathy is selective for low-SR fibers, particularly at high frequencies. As shown in

Figure 2·2, examination of fiber loss after acoustic trauma demonstrates a preferential loss of low-SR fibers, particularly above 4 kHz.

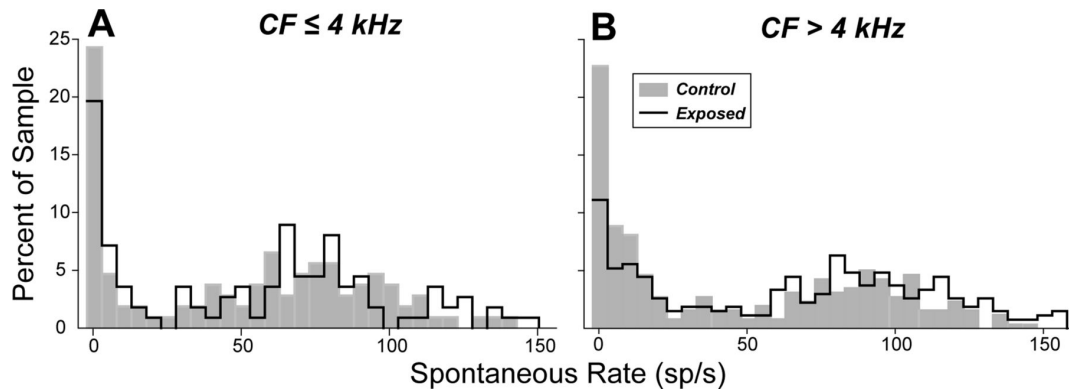


Figure 2·2: Synaptopathy is selective for fibers with low spontaneous rates, and particularly selective for low-SR fibers at high frequencies. Figure reprinted from Furman, Kujawa, and Liberman, 2013

2.3.3 Fiber SR Distribution is Not Tonotopically Uniform

Along the length of the basilar membrane, different percentages of low-, medium-, and high-SR fibers synapse on each IHC. Temchin et al., 2008; Temchin and Ruggiero, 2014; Bourien et al., 2014 have demonstrated in chinchilla and mongolian gerbil that there is a nonlinear distribution of low-SR fibers along the basilar membrane, with significantly more low-SR fibers per IHC at high frequencies. A distribution of fiber

rates per CF is given in Figure 2·3.

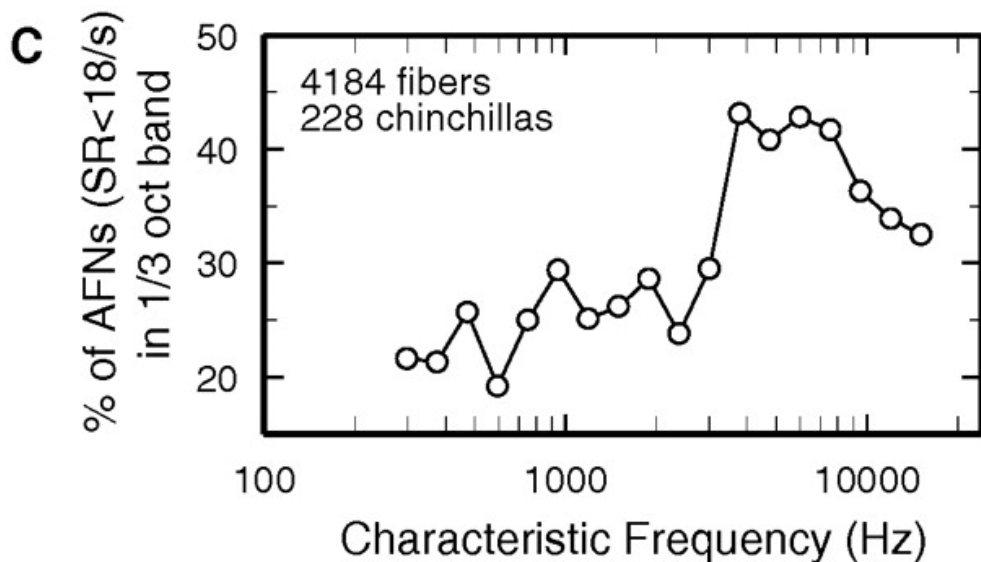


Figure 2·3: Distribution of Fiber Type. Conventional extracellular recording electrodes characterized the spontaneous rate of 4184 individual AN fibers in 228 chinchilla along the length of the Organ of Corti. Reprinted from Temchin, Rich, and Ruggero, 2008

2.4 Relevant Functional Neuroanatomy of the Auditory Mid-brain

Ascending from the AN, auditory information passes through multiple brainstem and midbrain areas en route to the thalamus, and then auditory cortex. A simplified schematic of sub-thalamic connections is given in Figure 2·4.

ABR Waves III and V are thought to reflect, in part, the synchronous contributions

of the Cochlear Nucleus and Inferior Colliculus. Therefore, it is important to consider both the effects of CS as well as more local physiology on the overall ABR.

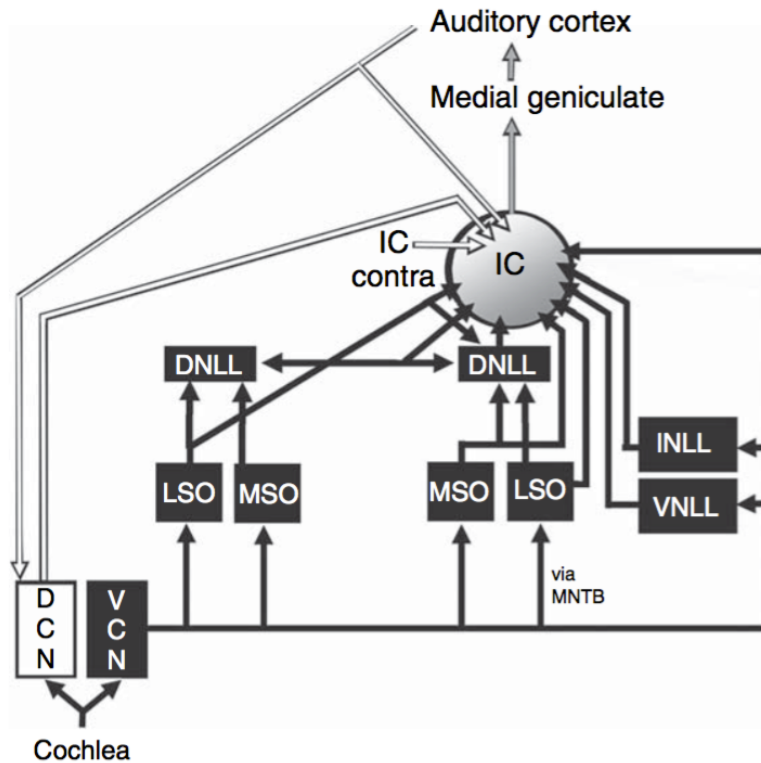


Figure 2·4: A simplified network diagram of the ascending auditory pathway in mammals. Pathways in white arise from the DCN; pathways in black from the VCN. Figure reprinted from Covey, 2008.

2.4.1 The Cochlear Nucleus

The primary projection from the AN is the Cochlear Nucleus, an inhomogeneous structure that is the first auditory relay station located in the ipsilateral medulla of the brainstem.

2.4.2 The Dorsal Cochlear Nucleus

Ryugo, 2008 demonstrated in cat that low-SR fibers have an anatomical projection bias towards the small cap of the Dorsal Cochlear Nucleus. While low-SR fibers project to many areas, the small cap receives input from low-SR fibers exclusively, suggesting a selective role for low-SR projections. Liberman, 1993 found similar results.

Further, while projections are selective as shown in Figure 2·5, the projections have relatively shallow but broad arbors. This anatomical specificity of projection combined with a breadth of coverage supports a particular role for low-SR fibers, and does not rule out the possibility of further specificities in higher brainstem and midbrain areas.

While the VCN is critically important for binaural processing, the specificities of projection observed in the DCN suggest an interesting role for synaptopathic losses that may be more monaural. Further, DCN projects directly to IC, whereas a proper consideration of contributions from the VCN would require a more involved treatment of pre-collicular regions such as the superior olivary complex (SOC).

2.4.3 The Inferior Colliculus

The IC has long been regarded as the last pre-thalamic obligate waystation for ascending auditory information, and a major center of pre-cortical auditory processing with many diverse functions (Cant & Benson, 2005; Covey, 2008; Moore & Kitze, 1985).

Recently, Beebe, Young, Mellott, and Schofield, 2016 has reported at least four morphologically different GABAergic neural types in IC that react in different ways to

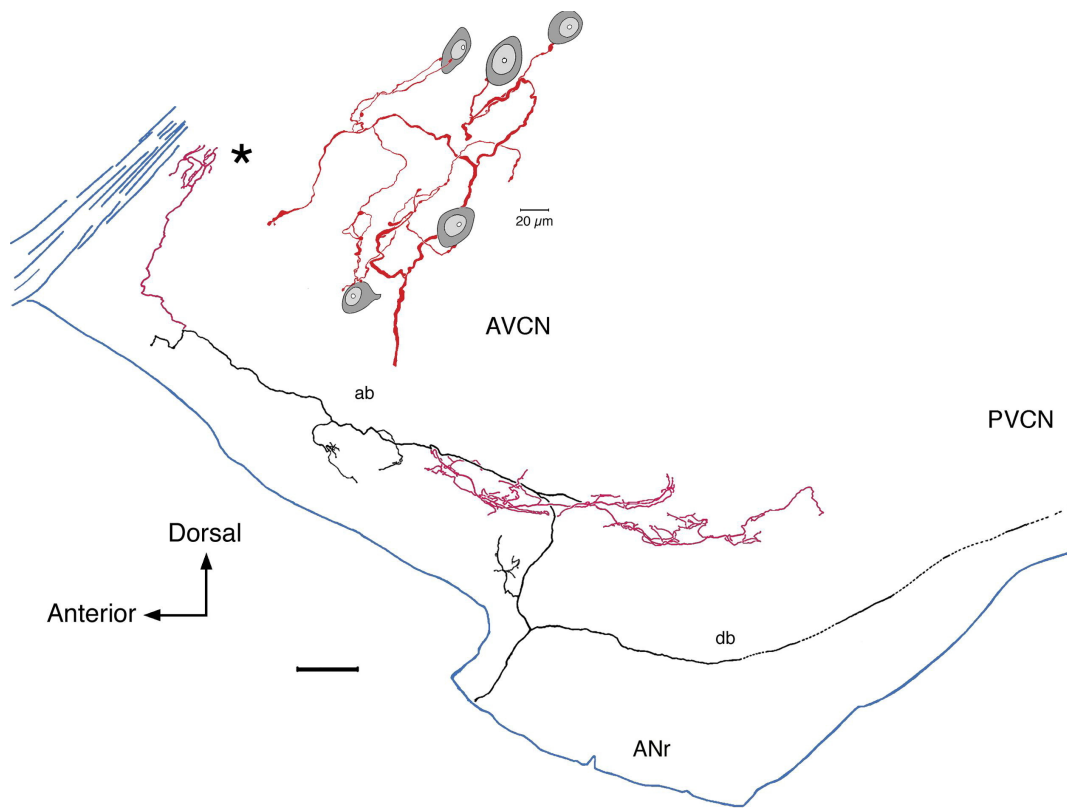


Figure 2·5: Low-SR fibers project to the Small Cap area of the DCN. From Ryugo, 2008, this shows a lateral view of a low SR fiber as it collaterizes (red) in the rostral and lateral SCC (CF=0.45 kHz; SR=1.2 s/s; Th=34 dB SPL).

auditory stimuli. Considering the recent diversity of IC responses that have been observed and will be discussed in subsection 2.6.2, this is a tantalizing anatomical observation that may correlate with electrophysiologically observed behavior.

2.5 Models of the Auditory Periphery

2.5.1 The Verhulst Model

A functional model of the auditory periphery was developed by Verhulst, Bharadwaj, Mehraei, Shera, and Shinn-Cunningham, 2015. As outlined in Figure 2·6, the model consists of a middle ear preprocessing model adapted from Meddis and Lopez-Poveda, 2010. Input is passed to a cochlear transmission line model, which estimates BM displacements and velocities for an arbitrary number of BM sections (default: 1000). Motions of the BM are translated into IHC bundle deflections and passed through a nonlinearity. Estimates of the Instantaneous Firing Rate (IFR) are made by a method adapted from Westerman and Smith, 1988, which implements a three-store diffusion model of synaptic vesicle and neurotransmitter release and reuptake. Unlike the Zilany model, the Verhulst model does not account for per-fiber noise in spontaneous rate.

The version of the model given by Verhulst et al., 2015 also includes a CN and IC modeling stage from Nelson and Carney, 2004, and the final model output are estimates of ABR Wave I, Wave III, and Wave V.

2.5.2 The Zilany and Bruce Model

Zilany and Bruce, 2006 proposed a phenomenological, signals-driven model of the auditory periphery. Since its creation, it has been regularly refined and updated to

Brainstem Response Model Overview

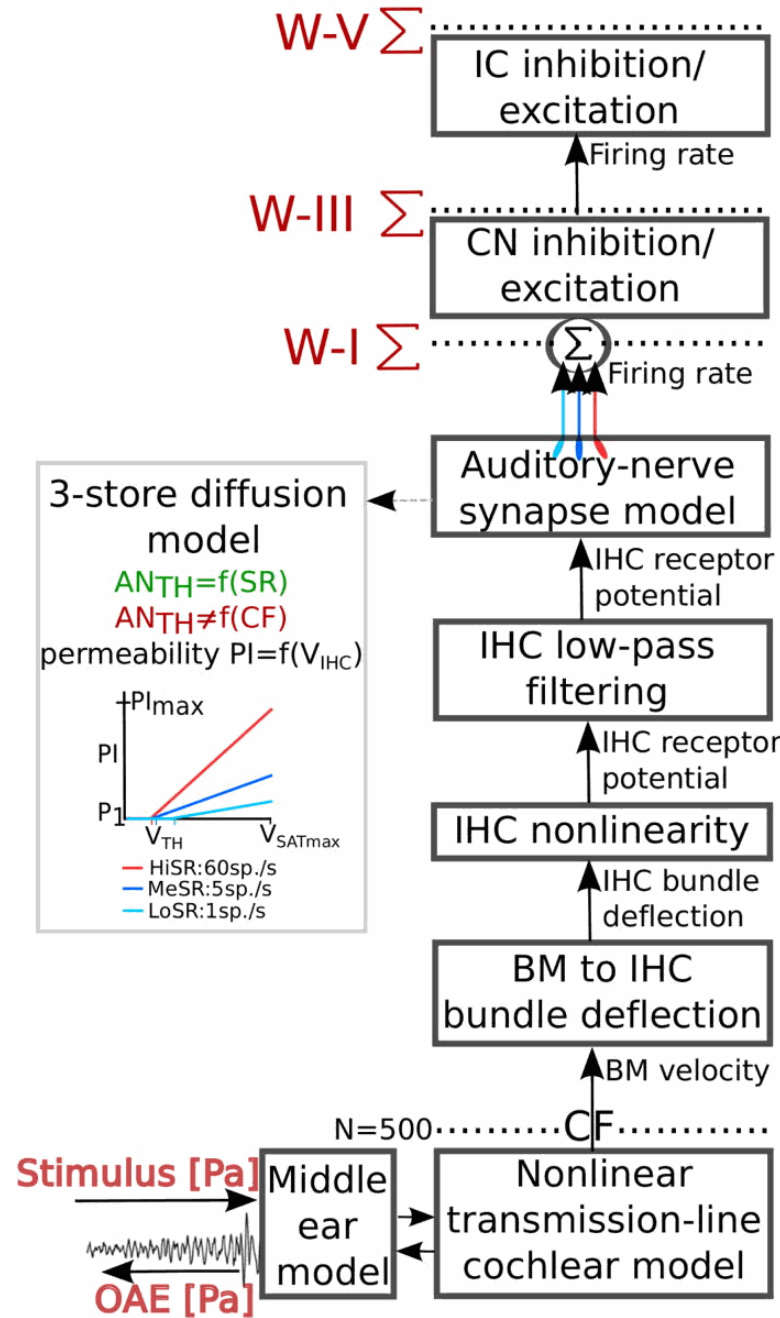


Figure 2·6: Major subunits of the Verhulst transmission line model of the auditory periphery. Figure is reprinted from Verhulst, Bharadwaj, Mehraei, Shera, and Shinn-Cunningham, 2015. Input (stimulus) and outputs (OAEs, Wave I, Wave III, Wave V) are in red, and located at their physiologically relevant levels.

account for an increasing number of phenomena including estimations of speech intelligibility (Zilany & Bruce, 2007), long-term IHC adaptation with power-law dynamics (Zilany, Bruce, Nelson, & Carney, 2009), and updates to more closely model human parameters (Zilany, Bruce, & Carney, 2014).

The approach is outlined in Figure 2·7 and consists of a phenomenological power-law model that has filters for each stage of the periphery. Fractional Gaussian noise is optionally added per-channel to simulate the stochasticity inherent in AN fiber spontaneous rates.

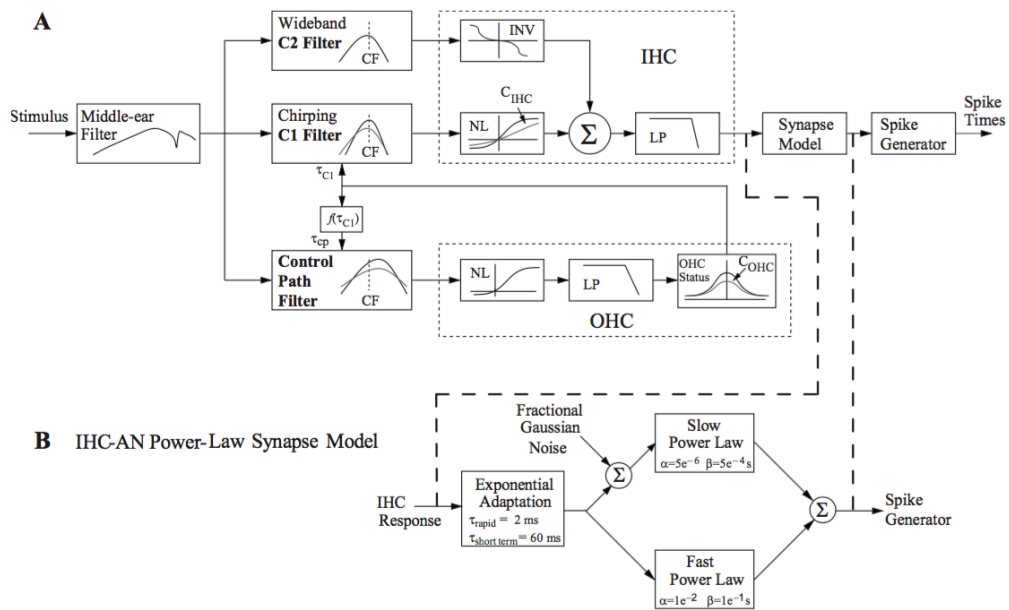


Figure 2·7: Major components of the Zilany model of the auditory periphery. Figure reprinted from Zilany, Bruce, Nelson, and Carney, 2009

2.6 Models of the Auditory Midbrain and Brainstem

2.6.1 The Nelson-Carney Model

Nelson and Carney, 2004 proposed a two-stage phenomenological model of the mid-brain and brainstem. The Cochlear Nucleus and Inferior Colliculus are each represented by a single Same-Frequency Inhibition Excitation (SFIE) filter, which convolves the output of the previous stage with excitatory and inhibitory alpha functions. As shown in Figure 2·8, these functions' delays, amplitudes, and onset times can be adjusted to provide a tuned response for a given unit, compared to electrophysiological measurements. In each case, each unit acts as a band-pass filter tuned to a certain bandwidth.

2.6.2 The Carney Model

Carney, Li, and McDonough, 2015 extended the two-stage Nelson and Carney, 2004 model by the incorporation of three categories of IC responses, compared with the single filter in subsection 2.6.1, to better account for processing of spectrally complex vowel tones. As shown in Figure 2·9, the IC is divided into three Same-Frequency Inhibition Excitation stages.

Based on electrophysiological recordings in awake rabbits, Figure 2·10 shows that Carney et al., 2015 represent 50% of the IC as band-pass responses, 25% as low-pass, and 25% as band reject filters. The weights were assigned based on the frequency of representation in IC.

This three-stage IC model more fully accounts for the neural diversities that have been observed anatomically by Beebe et al., 2016, and is robust at high sound level and at background noise levels.

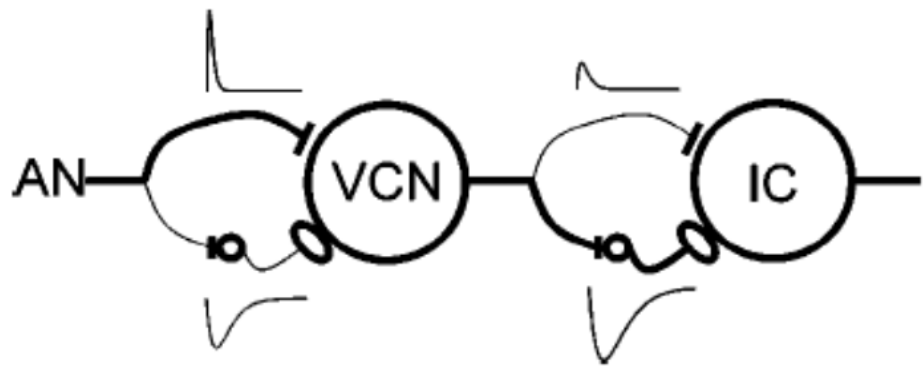


Figure 2·8: The Nelson and Carney Brainstem. Figure reprinted from Nelson and Carney, 2004.

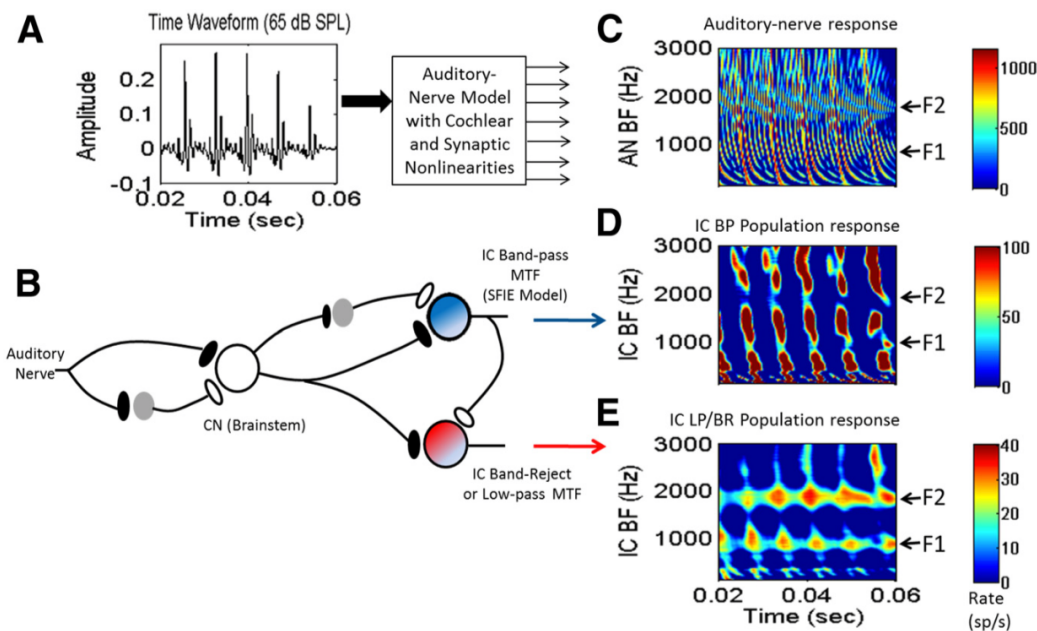


Figure 2.9: The Carney (2015) Midbrain and Brainstem. Figure reprinted from Carney, Li, and McDonough, 2015

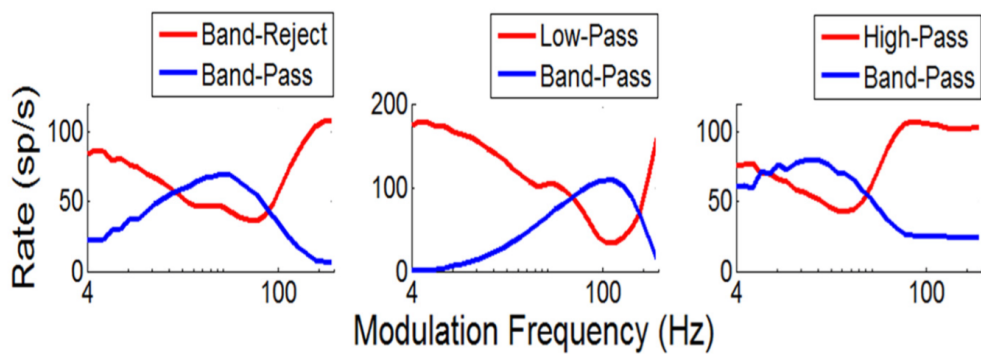


Figure 2·10: Different Response Types in the Carney Model. Figure reprinted from Carney, Li, and McDonough, 2015

2.7 The Auditory Brainstem Response

The Auditory Brainstem Response (ABR) is a powerful tool for noninvasive measurement of the function of different areas of auditory processing, from the auditory nerve to the auditory areas of the midbrain.

As outlined in Figure 2·11, the ABR is measured externally with scalp electrodes. A stimulus, often a click-train, is played monaurally. Over many repetitions, a characteristic waveform trace is obtained which represents the evoked potential generated by the synchronous activity of neural populations that respond to the stimulus.

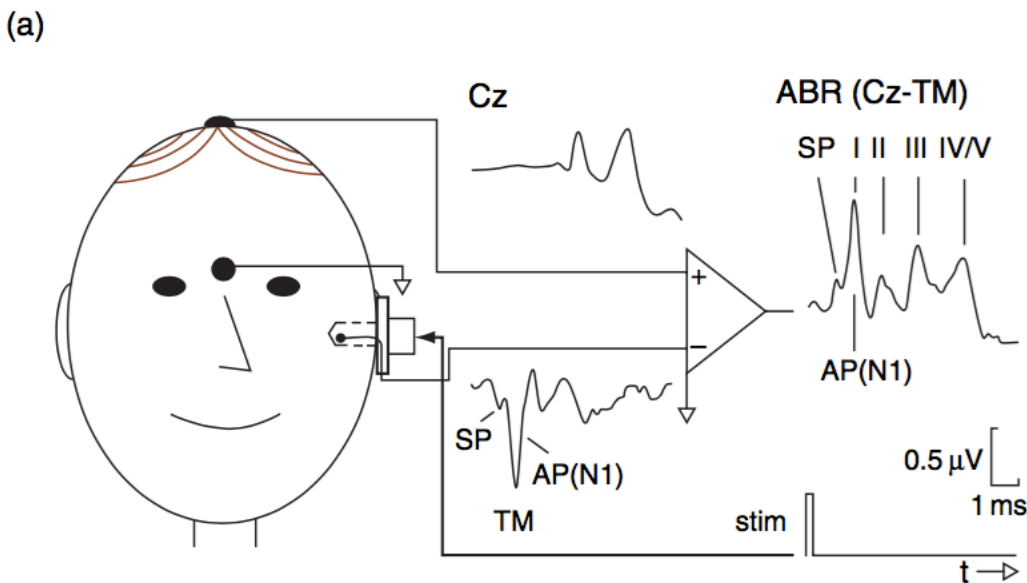


Figure 2·11: The Auditory Brainstem Response. Figure reprinted from Durrant, 2008

2.8 Candidate Objective Measures of Cochlear Synaptopathy in Humans

To date, there is no objective test in humans that would give definitive insight into whether or not a patient exhibits signs of HHL, or be able to quantify the degree or location of impairment.

Mehraei, 2015, in an attempt to direct the search for such a diagnostic, correlated performance in a psychophysical task with markers in ABR. In their work, 23 NHT listeners participated in a series of experiments to establish a relationship between task performance and putative cochlear synaptopathy. Cochlear mechanics function was validated with click-evoked OAEs. A behavioral measure of temporal sensitivity was established with an ITD envelope detection task with transposed tones. Noise-masked ABRs were measured with increasing noise level. As shown in Figure 2.12, Wave V latencies in increasing noise correlate with performance on ITD detection.

It is hypothesized that the combination of high sound levels used and broadband noise maskers for ABRs both preferentially drive low-SR fibers and recruit their resistance to background noise. Therefore, a synaptopathy-mediated decrease in low-SR fiber contributions would drive *down* the latency shifts observed.

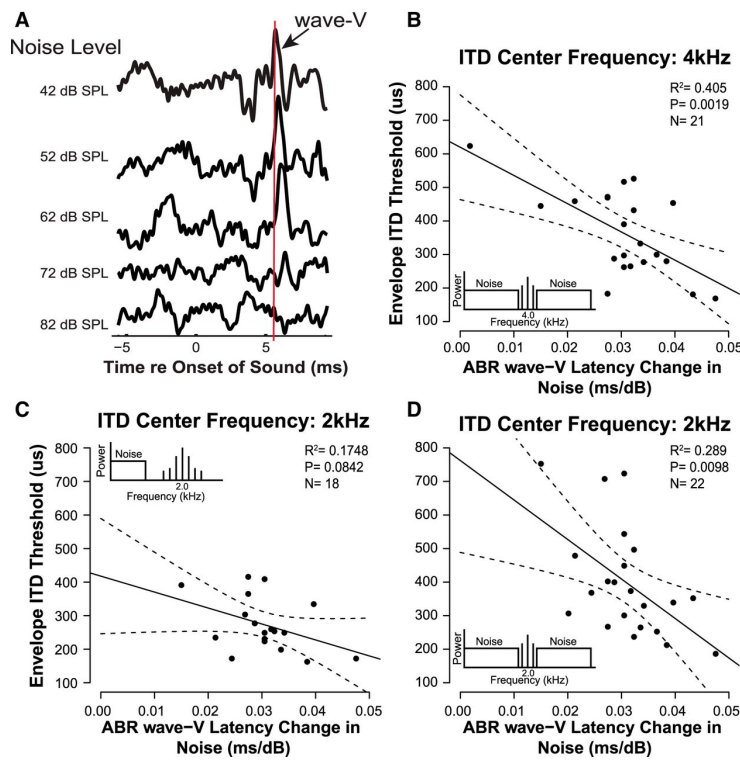


Figure 2.12: Wave V latencies in increasing noise correlate with performance on ITD detection. Figure reprinted from Mehraei et al., 2016.

Chapter 3

Aims

This thesis investigates several models of the peripheral and central auditory systems and the utility of their predictive abilities for cochlear synaptopathy in simulations of human audition.

Three aims were established. First, to develop a coherent modeling environment that combines models of the middle ear, auditory nerve, and auditory brainstem and midbrain from Zilany et al., 2014; Verhulst et al., 2015; Nelson and Carney, 2004; Carney et al., 2015 into one software package where the utility of each model could be compared head to head. Second, to advance the state of the models of the auditory periphery by extending them with new capabilities supported by available anatomical and physiological research. Third, to use the developed tool to explore the proposed mechanisms underlying psychophysical and large-scale electrophysiological studies of cochlear synaptopathy with higher fidelity.

3.1 Aim I. Simulate the ABR Response of a Noise-Masking Task with Variable SR Contributions and Model Parameters

A modeling environment was created. It incorporates two peripheral models of the auditory system: the Zilany model with humanized parameters (Zilany et al., 2014)

and the Verhulst model (Verhulst et al., 2015).

The Cochlea modeling environment (Rudnicki & Hemmert, 2014) was used to provide easy incorporation of the Zilany model into the new modeling environment. The transmission-line model of Verhulst et al., 2015, which has the potential to perform better in broadband noise due to its accounting for cochlear dispersion, was directly integrated. At the conclusion of this aim, direct comparisons between the estimates of ABR Wave I and Wave V by Zilany et al., 2014 and Verhulst et al., 2015 were performed for a variety of experimental conditions.

3.2 Aim II. Integrate Improved Brainstem Models

We hypothesized that the current approach to IC modeling taken in Verhulst et al., 2015; Mehraei et al., 2016 does not fully account for the responses to a low-SR knockout AN model, and consequently under-represents the effects on the ABR Wave V that have been experimentally measured.

In particular, an extension of the approach currently taken by Verhulst et al., 2015 was presented by Carney et al., 2015. It provides multiple classes of IC neurons that were shown to track complex tones (vowel formants) in noise. To guide the selection of model weights and connectivities, relevant neuroanatomical literature were consulted. Crucially, studies by Ryugo, 2008 and others have shown selectivities in SR projections to the small cap of the DCN, which will guide our modeling work by introducing specificities in weighting.

Further, while the latency change trend is preserved between both the models proposed by Zilany et al., 2014 and Verhulst et al., 2015, the magnitude of the effect is greatly different. This discrepancy may be remedied by introduction of new IC modeling components, which are better incorporated in the Zilany et al., 2014 model

3.3 Aim III. Relate Model Responses to Psychophysical Measures

We will compare subject Wave V latency data from Mehraei, 2015 and Mehraei et al., 2015 as ground truth to the improved model output. Interpreting the relative effects of different modeling parameters may elucidate which aspects of the auditory periphery are important in the further study of cochlear synaptopathy and its contribution to hidden hearing loss.

Chapter 4

The Corti Modeling Framework

4.1 Chapter Summary

This chapter gives a detailed description of the modeling environment created for this thesis. First, the configuration of the overall system is detailed. Second, the configuration and use of two models of the auditory periphery are detailed. Third, the creation of compound action potentials and population responses of the auditory nerve are given. A method for the simulation of cochlear synaptopathy is also detailed, along with a new incorporation of a nonlinear distribution of auditory nerve fiber types as a function of center frequency. Fourth, the use of these auditory nerve responses in simulation of the auditory brainstem and midbrain with two models are given, culminating in the creation of modeled Auditory Brainstem Responses. Finally, the utility of the system for large-scale simulation is shown.

4.2 Overview of Modeling Framework

The modeling framework created for this thesis has been named Corti (Voysey, 2016). It is architecturally inspired by the EarLab project developed at Boston University as well as the Cochlea (Rudnicki & Hemmert, 2014) modeling environment developed at the Technical University of Munich, from which it incorporates a peripheral model.

Corti is a command-line tool written in Python. As detailed in Figure 4·1, it is designed to produce estimates of the Auditory Brainstem Response, auditory nerve fiber, auditory nerve, brainstem and midbrain responses to an arbitrary stimulus. A set of configuration parameters determine which models are used and how they are interconnected, as well as the spatiotemporal properties of the stimulus.

4.2.1 Software Design

Corti has been designed to be an easy to use and flexible command-line tool that should be immediately usable to anyone interested in auditory modeling who is familiar with basic auditory physiology and engineering. It has a fully documented user interface, requires no special system configuration to use, and runs on Linux, Windows, and OSX.

Corti is publicly available and open source, licensed under the GNU GPLv3. It is free to distribute, use, and be contributed to by anyone. The file format used to store large simulation output is the Hierachal Data Format (HDF5), which is a database in a file that can be analyzed and accessed by any operating system and any modern programming language—while Corti is written in Python, analysis of its output may be done in MATLAB, R, SPSS or any other modern data analysis tool.

Corti was designed so that its output can be easily audited and examined to know not only which biophysical parameters were used, but also know comprehensive metadata about the simulation itself. For example, model output contains which version of each model was used, the date and time of the computation, a copy of the stimulus used to stimulate the models, and a comprehensive record of other relevant parameters.

Additionally, the development history of Corti is publicly accessible on the collaborative software repository website GitHub (<https://github.com/gvoysey/corti>). Every

change made, and every version released, is available so direct comparisons between output can be made, and software bugs fixed in a central location. A permanent archive of the version of Corti described in this thesis has been assigned a Document Object Identifier (DOI), and is available via Zenodo, which is an EU and CERN funded research data repository. At the time of this writing, Corti has been used to run simulations by research groups at Boston University, the Massachusetts General Hospital, the Carl von Ossietzky University of Oldenburg, and the Technical University of Denmark.

4.2.2 Configuration Options Define a Parameter Space

As detailed in chapter 2, the constituent models of this framework each require many choices of user-selected parameters, ranging from sampling frequency to the time constants and relative strength and latency of inhibitory and excitatory contributions of brainstem areas. Several other parameters are introduced in the framework itself, as well as the choice of which model to use for each stage. Because these parameter choices directly modulate the simulation output, it quickly becomes natural to treat these different options as a high-dimensional parameter space. Any single run of the framework, using one collection of options, defines a particular trajectory through this space.

4.3 Simulation using Corti

As shown in Figure 4·1, a full simulation using Corti involves three primary processing stages: the Peripheral, Auditory Nerve, and Brainstem / Midbrain. The next sections of this chapter will treat each stage in detail.

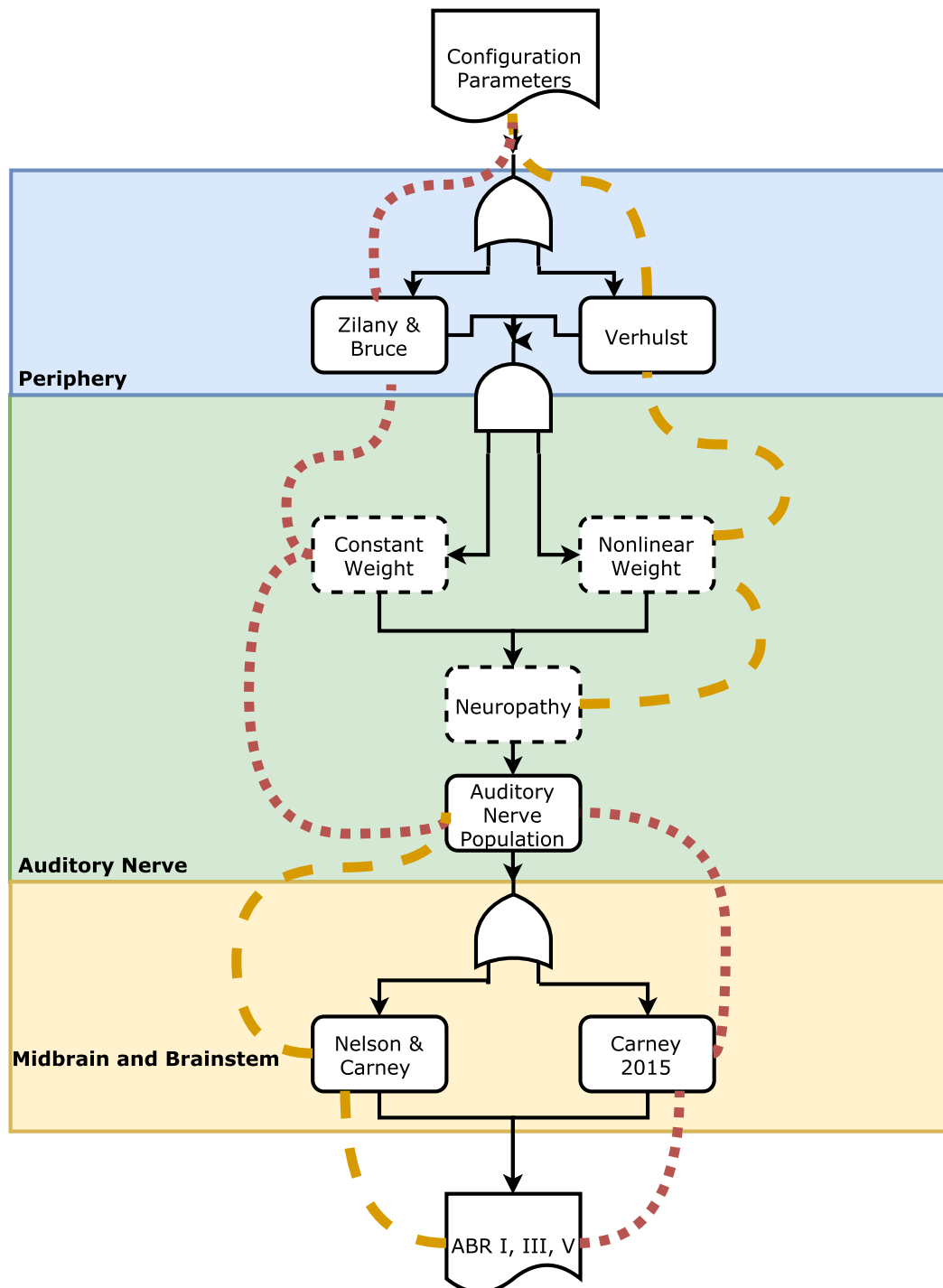


Figure 4·1: Overview of the Corti modeling environment. Two parameter trajectories are shown: a simulation of auditory neuropathy using the Verhulst periphery, nonlinear weights of fiber type contributions, and the Nelson and Carney brainstem (orange), and a simulation without neuropathy using the Zilany periphery, linear fiber weighting, and the Carney 2015 brainstem (red).

4.4 Peripheral Models

The Peripheral stage takes a stimulus and produces estimates of the Instantaneous Firing Rate for three fibers per CF. Two models of the auditory periphery are included: the transmission-line model by Verhulst et al., 2015 (henceforth “The Verhulst model”) and the phenomenological model by Zilany et al., 2014 (henceforth “The Zilany model”). This section corresponds to the first stage of Figure 4·1, highlighted in blue.

As detailed in Figure 4·2, both models simulate the response of the peripheral auditory system to a pressure wave, and both produce time-series estimates of Instantaneous Firing Rates (IFRs) for an arbitrary number of inner hair cells which are tonotopically distributed along the length of the basilar membrane via the Greenwood function.

4.4.1 The Verhulst Model

The Verhulst model is particularly well-suited for modeling broadband stimuli. Since it is a transmission line model which gives estimates for the position and deflection of the entire basilar membrane even to a pure tone stimulus, it naturally accounts for dispersive effects, and produces detailed information about many stages of sound propagation. Though not used in this work, the Verhulst model is also capable of modeling Otoacoustic emissions in response to complex stimuli.

Since the development of the Verhulst model is still underway, it has been programmatically isolated in a separate package. This provides a separation of concerns between the projects, and allows both Corti and the Verhulst model to be updated independently of each other as new features are made available in both.

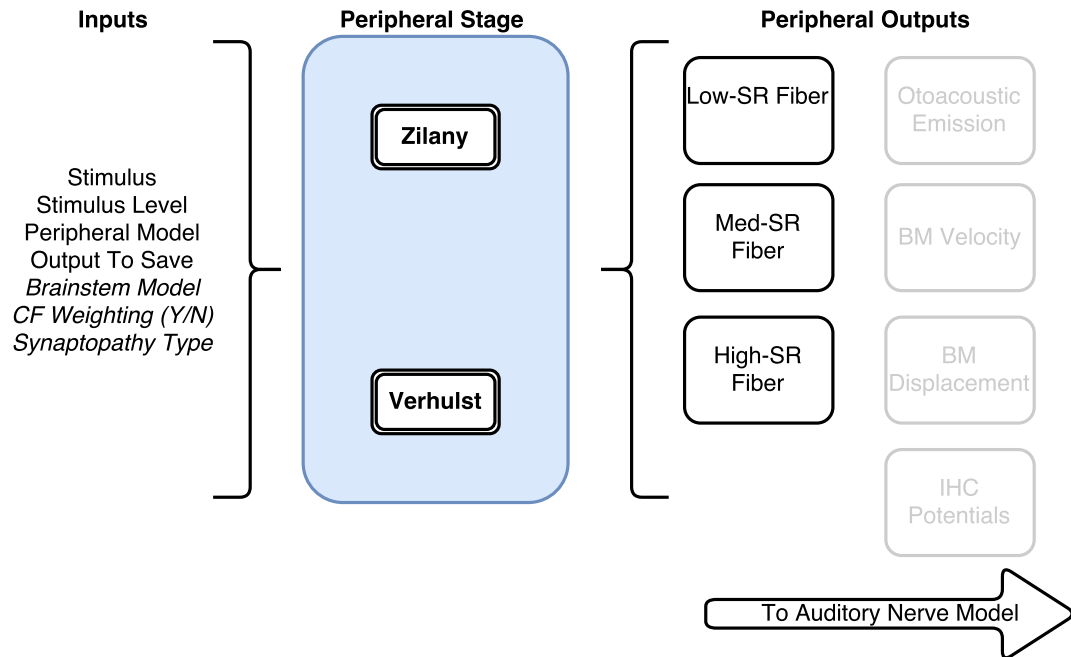


Figure 4·2: The Peripheral stage. All model inputs are shown; inputs in italics are used in later stages. Three estimates of fiber IFRs are always produced (in black text), and are passed to the Auditory Nerve modeling stage. In grey, the Verhulst model may also produce other output which can be optionally stored, but is not used for ABR estimation.

4.4.2 The Zilany Model

The Zilany model is a very commonly used model of the auditory periphery, and robustly accounts for many phenomena observed electrophysiologically to complex stimuli. The model was originally developed based on measurements in cat (Zilany & Bruce, 2006), and has since been updated to account for spectrally complex sounds via power-law adaptation (Zilany & Bruce, 2007) and later with humanized parameters to better reflect psychophysical data (Zilany et al., 2014).

The implementation of the Zilany model here was adapted from Rudnicki and Hemmert, 2014, who provided a Python and C implementation that has been shown to produce identical output to the version documented by Zilany et al., 2014.

4.4.3 Accounting for Variations in Spontaneous Rates Between Models

While both the Zilany and Verhulst models produce estimates of the instantaneous firing rate of the auditory nerve, the means by which they do so are different enough that care must be taken in directly comparing their estimates.

The classification of SR types by mean spontaneous firing rate differs between the Zilany and Verhulst models. The Zilany model defines a low-SR fiber to have a spontaneous rate of 0.1 spikes/second, a medium-SR fiber to have a spontaneous rate of 10 spikes/second, and a high-SR fiber to have a rate of 100 spikes/second. The Verhulst model defines these values as 1, 10, and 60 spikes/second, respectively. As discussed in subsection 2.3.2 and subsection 4.5.3, Temchin et al., 2008 combine low- and medium-SR fibers into one population and define it to have a spontaneous rate of less than 18 spikes/second. For the purposes of this work, both the Zilany and Verhulst model support this approach.

Therefore, while both the Verhulst and Zilany model support classification of spontaneous rates into three categories, for the purposes of weighting fiber types both low- and medium-SR populations may be treated identically.

4.4.4 Peripheral Model Output

The Verhulst model provides estimates of response behavior at many stages of the of the auditory periphery. For models of motion in the middle ear, estimates are computed for each basilar membrane section. By default, the BM is divided into 1000 section. Each section corresponds to one CF, where the place-frequency map is obtained via the Greenwood function.

While running the simulation, the following model outputs may be stored to disk for further analysis:

1. Basilar membrane velocities for each section.
2. Basilar membrane displacements for each section.
3. Inner hair cell receptor potentials.
4. IFR for a high spontaneous rate fiber.
5. IFR for a medium spontaneous rate fiber.
6. IFR for a low spontaneous rate fiber.
7. The Otoacoustic emission.

The Zilany model, as implemented, provides IFR estimates only. Hair cell potentials could also be modeled, but are omitted.

Both models provide estimates of Instantaneous Firing Rate as a function of post-stimulus time for each combination of fiber type and best frequency, and these are

passed to the next stage of the Corti environment.

4.5 Auditory Nerve Response Models

This stage of processing converts IFRs of specific fiber populations made by either the Zilany or Verhulst model into an estimate of the summed activity of the auditory nerve. It corresponds to the green-shaded region of Figure 4·1, and is outlined in detail in Figure 4·3. Depending on the parameters chosen, output of either the Zilany or Verhulst peripheral models are first summed into a population response of the AN by one of two means. Next, degradation of the population response that corresponds to a model of synaptopathy is applied; finally, the summed population response is passed to the midbrain and brainstem models.

4.5.1 Modeling the Contributions of Inner Hair Cells

The output of the Zilany and Verhulst peripheral models are IFRs for one stereotypical AN fiber of each SR type per CF. However, tens of fibers synapse on each IHC along the length of the cochlea. Consequently, to generate an estimate of IFR per CF or per BM section, each stereotypical AN fiber must be scaled by some weighting factor so that its output becomes an estimate of the summed IFRs of its SR category for a given IHC. Based on anatomical data (Liberman, 1978), the Verhulst model assigns 19 fibers to each inner hair cell. The Zilany model makes no inherent assumptions about number of fibers per IHC, so to maintain equivalence with the Verhulst model and allow like-to-like comparison of model output, IFR estimates from both models are distributed among 19 fibers.

In Figure 4·1, this process is the first contribution of the AN processing area in green, and is accomplished by either a constant or nonlinear weight.

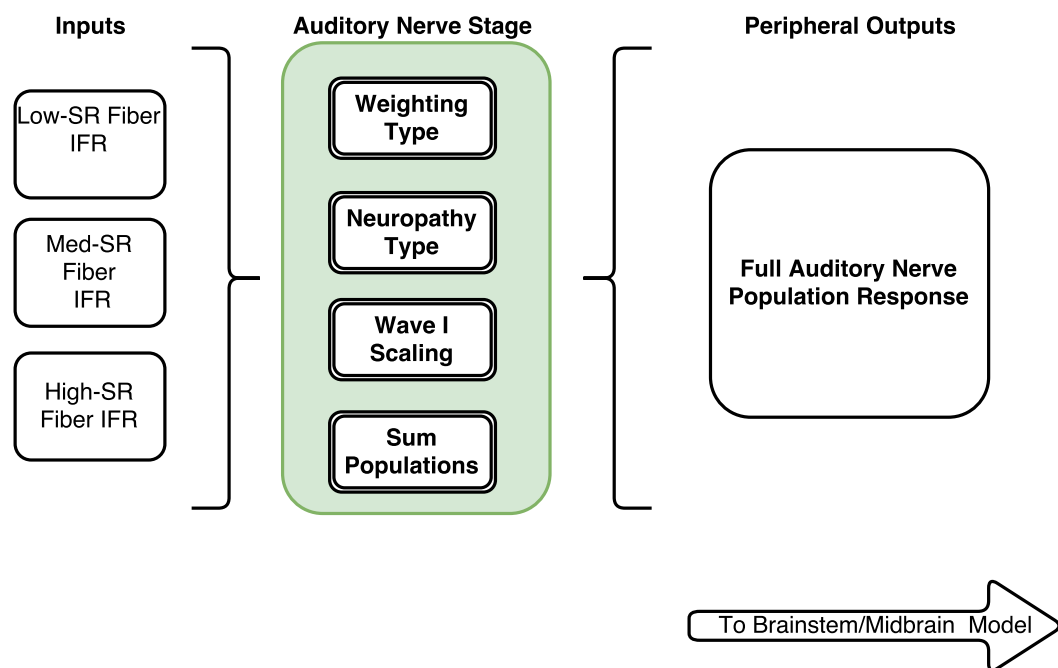


Figure 4·3: The Auditory Nerve Stage. Single IFR estimates for fiber types at each CF are weighted to produce an estimate of the total IFR at each IHC/CF. These are optionally degraded to model synaptopathy, weighted to produce physiologically appropriate Wave I amplitudes, and summed into the total population response of the Auditory Nerve.

4.5.2 Weighting of IHC contributions

To determine which proportion of the total contribution of a given hair cell arises from fibers of a given spontaneous rate, the Verhulst model applies a scalar weighting factor to the summed Auditory Nerve Response using an undamaged nerve with 19 total fibers. Three fibers are assigned for low- and medium- SR fibers and 13 for high-SR fibers per hair cell.

Once each hair cell's contribution has been computed and summed into the total response, a scalar weighting factor was empirically chosen such that the modeled and summed response of IHCs with CFs between 175Hz and 20kHz produces a model ABR Wave I amplitude of $15 \mu\text{V}$. For the Verhulst model, Verhulst et al., 2015 found the value of this weighting factor to be $0.15\text{e}{-6} \text{ V} \times 2.7676\text{e}{-7}$. This weighting factor is given as a product to emphasize that it directly fixes the peak Wave I output at $15\mu\text{V}$.

To produce comparable results in this work, the Zilany model was scaled accordingly. We iteratively converged on a scaling factor that produced an ABR Wave I amplitude of $15\mu\text{V} \pm 1\text{nV}$, which was found to be $0.15\text{e}{-6} \text{ V} \times 7.30282\text{e}{-7}$.

4.5.3 Weighting of Fiber Types per IHC

Based on data from Temchin et al., 2008, and as reviewed in section 2.3, the distribution of SR fiber types per IHC may not be uniform along the length of the basilar membrane. To account for this, we have extended the linear distribution of fiber types per hair cell with the option of a logistic distribution as a parameter. As shown in Figure 4.4, experimental data for SR distribution as a function of CF was fitted via logistic regression in MATLAB, and this regression function was used to generate an empirical estimate of SR type.

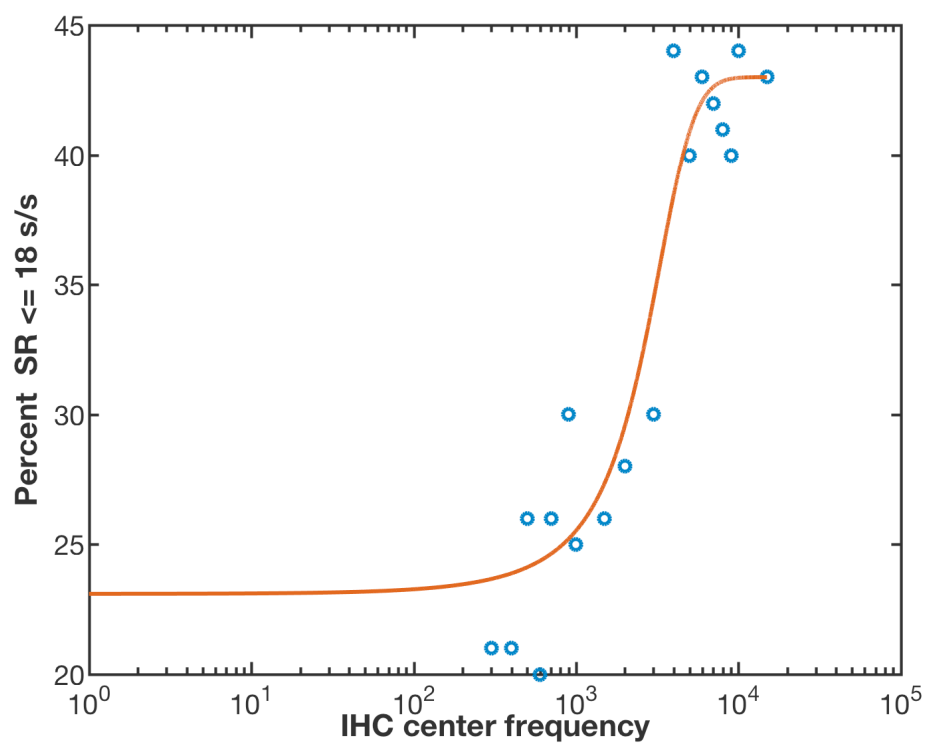


Figure 4·4: Experimental results (blue circles) reported by Temchin, Rich, and Ruggero, 2008 were fit to a logistic model (red solid line).

The empirical logistic fit equation that estimates p , the percentage of fibers with spontaneous rates below 18 spikes/sec innervating a given inner hair cell as a function of best frequency was found to be:

$$p(cf) = 21 + \frac{k}{1 + e^{-r \cdot (cf - cf_0)}} \quad (4.1)$$

where $k = 22$, $r = 9e-6$ and $cf_0 = 2500$.

Fractional Weights

A consequence of the IFR weighting approach taken here is that while the total fiber count per IHC is fixed at 19 fibers, the percentage of the summed response of that IHC that arises from a given fiber type is not guaranteed to represent an integer number of fibers. For example, a CF of 8 kHz has 42.9 percent of its innervating spiral ganglia with spontaneous rates below 18 spikes/second, or a total of 8.133 low and medium spontaneous rate fibers.

Therefore, it is appropriate to think of the modeled IFR values as the weighted contributions of a SR type to the overall IFR originating from a particular CF, rather than the summed responses of integer numbers of individual fibers. In the context of producing auditory nerve responses—as are used in this work—this can be thought of as providing a more accurate representation of *summed* physiological responses. Model responses of unitary fibers of different spontaneous rates are saved in the peripheral output, if desired.

4.5.4 Modeling Synaptopathy

Cochlear synaptopathy is the loss of the synapse between an inner hair cell and an individual spiral ganglion. At the level of the summed auditory nerve response, selective degradation is modeled by reducing the contribution of each fiber type per hair cell by a scaling factor.

Six predetermined severity levels, as given in Figure 4·5 were chosen to model cochlear synaptopathy, all of which behave similarly. In each case, the portion of the response from a hair cell of a given center frequency is scaled by a percentage of its magnitude before being summed into the auditory nerve response.

Synaptopathy Type	Percentage Degradation		
	lowSR	medSR	highSR
none	0	0	0
mild	10	10	10
moderate	25	25	25
severe	50	50	50
ls-mild	10	10	0
ls-moderate	25	25	0
ls-severe	50	50	0

Figure 4·5: The default types of cochlear synaptopathy that may be simulated. The percentage by which the IFRs of a given fiber type are reduced are given in each row. In the case of the Low SR (ls) synaptopathies ls-mild, ls-moderate, and ls-severe, only the low- and medium- SR fibers are degraded.

4.6 Brainstem Models

This section details the two brainstem models in use, given by Nelson and Carney, 2004 and Carney et al., 2015. These correspond to the yellow region of Figure 4·1, and are detailed in Figure 4·6.

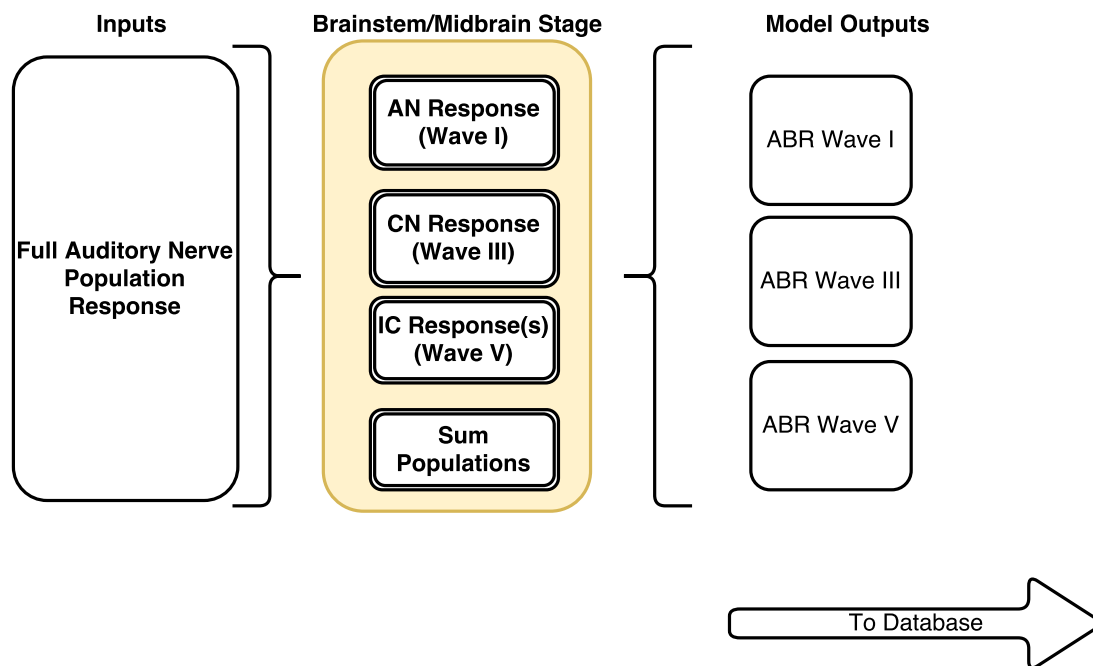


Figure 4·6: The Brainstem and Midbrain stage. The summed Auditory Nerve population response is convolved with Same-Frequency Inhibition/Excitation models to produce estimates of the Cochlear Nucleus response. Wave I estimates are made from the AN response. The response of the IC is simulated with one or three SFIE model(s), depending on which brainstem model was chosen. From the CN and IC responses, estimates of Waves III and V are made.

4.6.1 Choice of Best Modulation Frequency

The included models of the CN and IC are tuned to a best modulation frequency (BMF)—i.e., the stimulus modulation frequency at which they have a peak response—of 100 Hz, as this was found by Carney et al., 2015 to be the most relevant modulation

frequency for speech-like complex sounds such as vowel formants. These responses thus may be regarded as Modulation Transfer Functions (MTF). It is not clear the extent to which the CN or IC possess a “MTF filter-bank”, where units are tuned to multiple BMFs, so this has not been implemented.

4.6.2 The Nelson Carney 2004 Brainstem

In the case of the simpler brainstem and midbrain model of Nelson and Carney, 2004, the CN and IC are both represented as single processing stages where an excitatory and inhibitory alpha function are convolved with, in the CN, the ANR population response, and in the IC, the output of the CN stage.

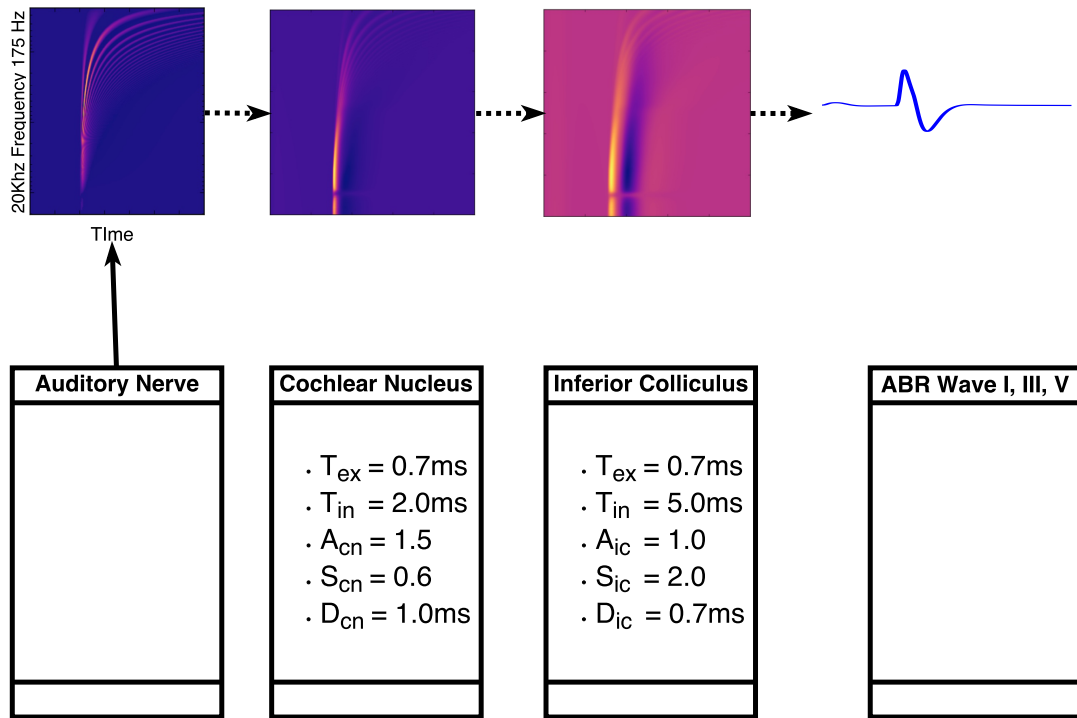


Figure 4·7: Overview of the processing stages of the Nelson-Carney brainstem model and model output at various stages for an 80dB click stimulus. Coefficients, which define the excitation and inhibition onset times and amplitudes for the CN and IC, are given.

4.6.3 The Carney 2015 Brainstem

In the case of the more complex model proposed by Carney et al., 2015, the IC processing stage incorporates three types of filters, which better reflect the diversity of neural responses observed electrophysiologically.

Weights of contribution for each type are as shown in Figure 4·8, and were chosen to represent the relative magnitudes of effect observed by Carney et al., 2015 in electrophysiological study. Weighing is uniform across center frequency.

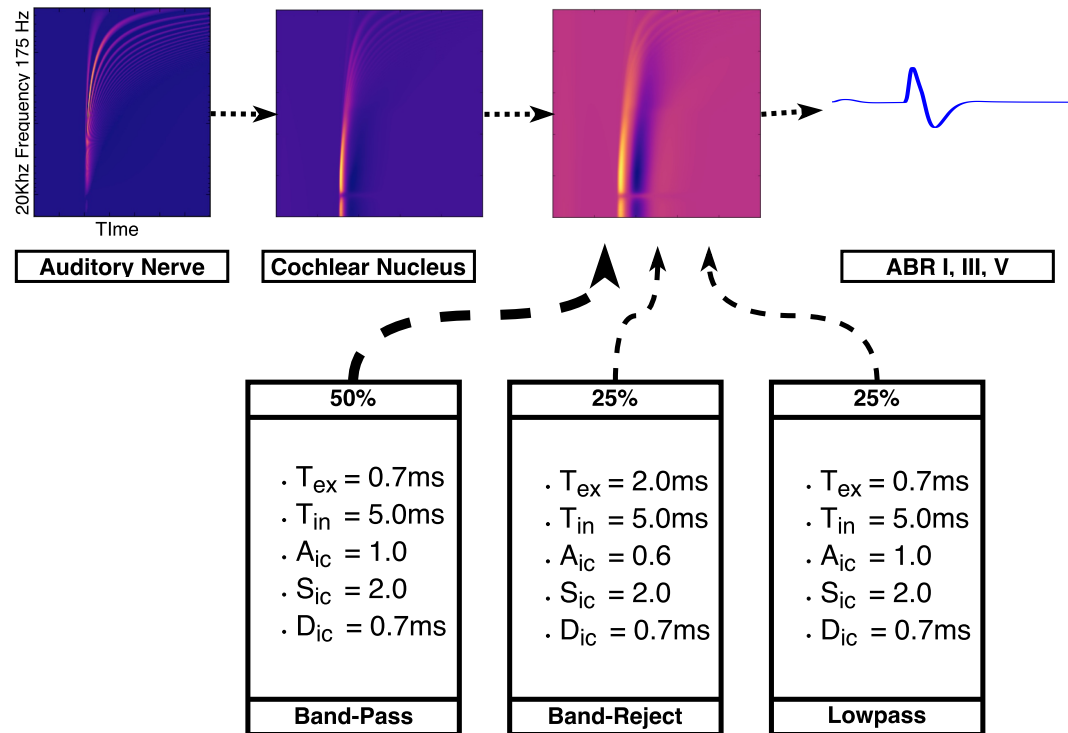


Figure 4·8: Overview of the processing stages of the Carney, Li, and McDonough, 2015 brainstem model for an 80dB click. Coefficients and weights for the three-stage IC model are shown; other parameters are as in Figure 4·7

4.7 Stimulus Generation

Corti supports simulations of stimuli of arbitrary duration and level. Simple stimuli such as clicks are generated programmatically by specifying a series of parameters such as onset time and duration.

More complex stimuli can be created and passed in as WAV files. All WAV stimuli must specify the sound level, in dB SPL re $20\mu\text{Pa}$, at which they should be presented; the waveform is then normalized by the peak value (in the case of a click) or the RMS value (for spectrally complex stimuli) and rescaled to have units of Pascals prior to simulation.

4.8 Automated Parameter Exploration

Corti may be run in one of two modes. In the first, a single set of parameters defines a single trajectory and the model is run once. However, while this mode of operation is convenient for fast simulations whose parameters can be defined *a priori*, it rapidly becomes impractical for situations where the relative effects of different parameter choices are to be compared, and reliable book-keeping of which parameters were used to generate which results becomes unnecessarily challenging.

Therefore, a second means of use was created, as detailed in Figure 4.9. The core of this mode is the Python Parameter Exploration Toolkit (Meyer & Obermayer, 2016). It provides the tools to allow a convenient interface to explore the parameter space generated by the specification of many available models, impairments, and options in a manner that allows easy *post-hoc* analysis. Individual trajectories may be computed in parallel on a single workstation or in a high-performance cluster so that the relative effects of each model, neuropathic impairment, and other features

may be directly compared. The results for all combinations of model components are stored in one Hierarchical Data Format (HDF5) file. Comparisons of the effect of using different trajectories to the same stimuli can then be made in a way that guarantees an internally consistent analysis.

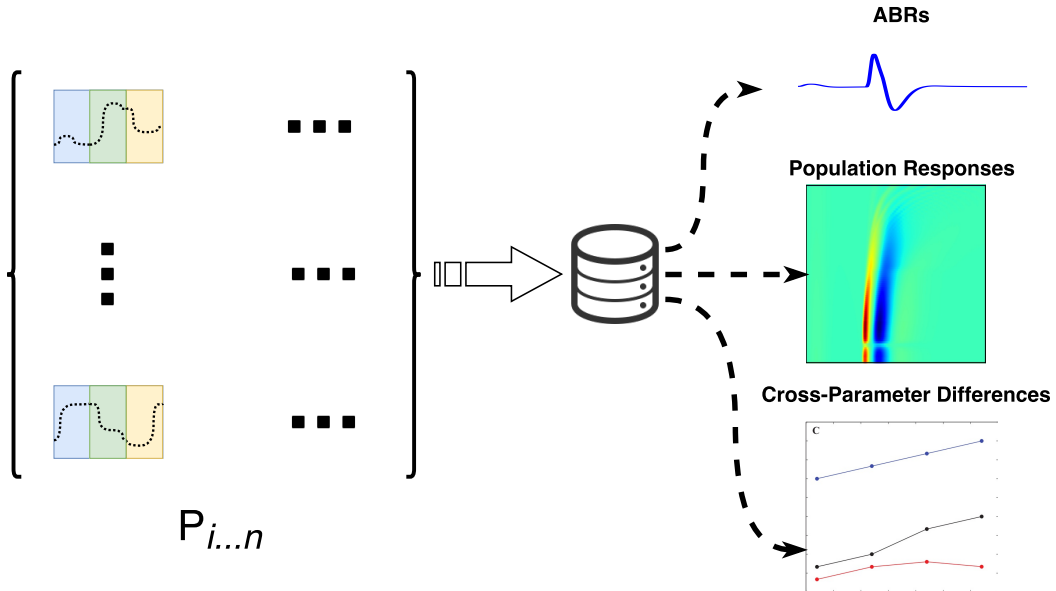


Figure 4.9: Automated exploration of model parameters P_i is one set of multiple parameter values required to specify one trajectory. A total of N trajectories, where N is the Cartesian product of the specified value ranges that a given parameter may take, are computed in parallel and stored in a database for further analysis.

4.8.1 Design of New Experiments

While chapter 5 focuses on a particular combination of trajectories, designed to replicate and explore the contributions of different modeling considerations to a particular stimulus, the method presented in section 4.8 is much more generally applicable. Using Corti, one can easily design and run many other modeling experiments using these techniques for a wide variety of stimuli or parameter values without modification of the code of the core model functionality.

Chapter 5

Results

5.1 Chapter Summary

This chapter describes the results obtained when using the modeling environment described in chapter 4.

5.2 Modeling a Human Noise-Masked ABR

The model ABR in response to a click-train in noise was computed for a variety of masker ratios. The experiment design tool described in section 4.8 was used to specify a range of values for each parameter in Corti to reveal the relative contributions of each.

5.3 Quantification of Model Changes are Level Sets

Five free parameters—stimulus, peripheral model, brainstem and midbrain models, synaptopathy, and IHC weighting—were varied over the course of all simulations.

Quantification of single parameter changes can be best accomplished by considering the effect of a change of the value of an individual parameter while all others are held constant. In this way, the level set of the parameter space may be considered.

In all cases, the effects of a parameter change is of interest for the same two objective measures: Wave I amplitude, and Wave V latency change. Consequently, visualization of each level set is most intuitive by projecting it onto those axes.

5.3.1 Stimuli

Following Mehraei, 2015; Mehraei et al., 2016, six stimuli were programmatically generated and stored as WAV files with a sampling frequency of 100 kHz. As shown in Figure 5·1, stimulus onset was delayed by 20 μ s of silence, and then consisted of 80 dB SPL clicks with a repetition rate of 100 ms in the presence of Gaussian noise at different signal to noise ratios.

Importantly, these stimuli are all well above the threshold of audibility; the aim is to obtain a response of the auditory models as they react robustly to a clearly audible input.

All other parameters values—choice of peripheral and brainstem model and logistically weighted fiber distributions—were fully explored.

In total, 240 separate simulations were run in parallel on Boston University’s high-performance computing cluster over the course of approximately 9 days. Model output was automatically stored into a HDF5 database approximately 250 GB in size.

5.4 Effect of Cochlear Synaptopathy

The effects of four types of synaptopathy—moderate, severe, low-SR specific moderate, and low-SR specific severe—were simulated, with the synaptic degradation parameters as given in Figure 4·5.

The effect of fiber loss on Wave V peak latency and Wave I peak amplitude for all

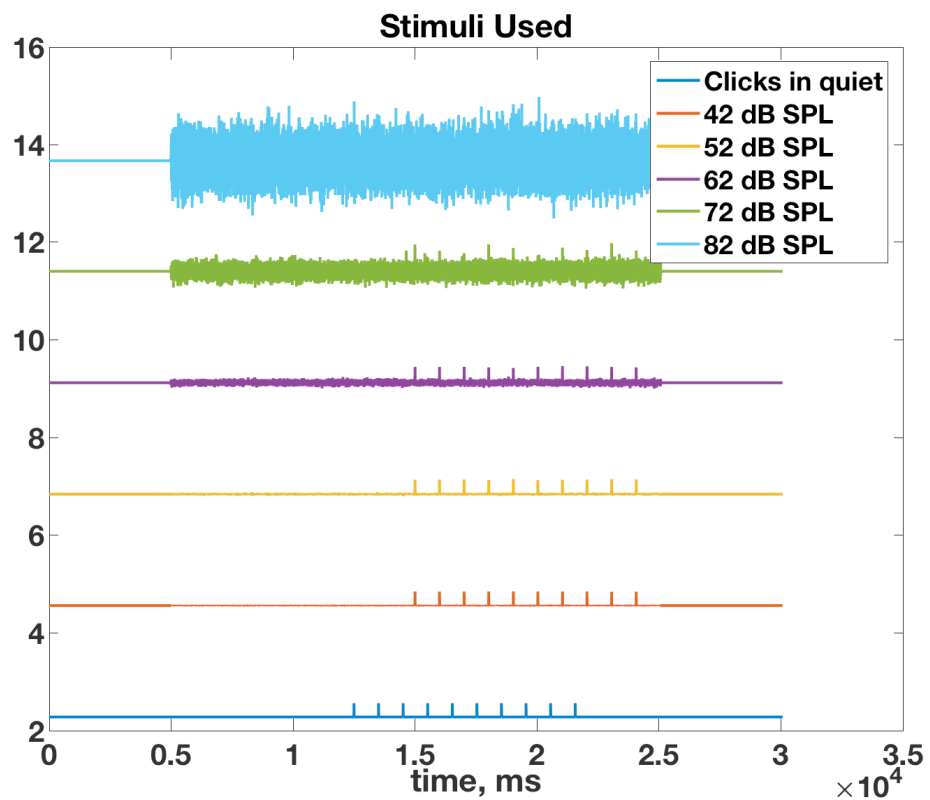


Figure 5·1: Stimuli used to drive the auditory models. All stimuli were an 80dB SPL click train with a 100ms spacing between clicks. A white Gaussian noise masker was added at five different masker levels.

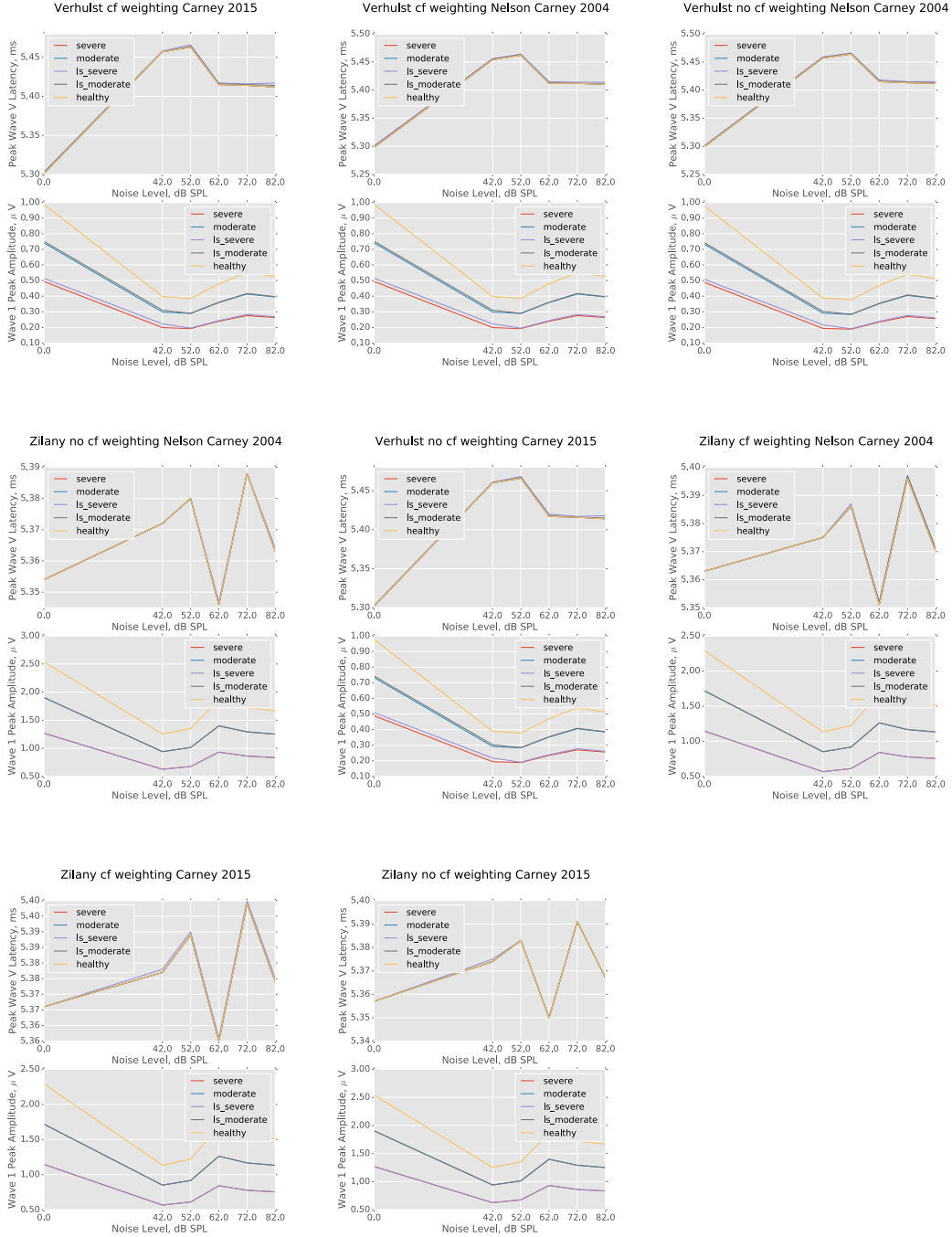


Figure 5.2: The effects of varying degrees of synaptopathy on model responses to a stimulus at multiple noise levels. Some traces are present but not visible as they precisely overlay other results.

other parameter combinations are given in Figure 5·2.

Consistent with prediction and prior experiment, Wave I amplitudes decrease as a function of synaptopathy, as well as a function of increasing noise masker level. Selective loss of low SR fibers closely follow their corresponding all-fiber degradation models, suggesting that low-SR degradation at the simulated severities don't contribute towards amplitude changes in the presence of high level noise maskers.

Wave V latencies exhibit a consistent increase in latency relative to a pure click train, consistent with observations by Mehraei et al., 2016, but latency magnitudes are not significantly affected by modeled synaptopathy.

5.5 Effect of Peripheral Model Choice

Because we observe little difference in the Wave I and Wave V responses as a function of the types of synaptopathy modeled in section 5.4, the relative effects of peripheral and brainstem model types can be explored while holding the type of synaptopathy fixed. This temporarily removes one dimension of the parameter space.

The effects of peripheral model choice on Wave V peak latency and Wave I peak amplitudes are given in Figure 5·3. In general, the Verhulst model predicts both larger Wave V latencies and larger changes as a function of SNR compared to the Zilany model, which predicts generally small to no change in latencies. This is contrary to earlier modeling results, which suggest the opposite effect of peripheral models.

Wave I amplitude estimations follow similar shapes for each peripheral model. While both produce physiologically plausible responses, the Verhulst model predicts amplitudes approximately half the magnitude of the Zilany model.

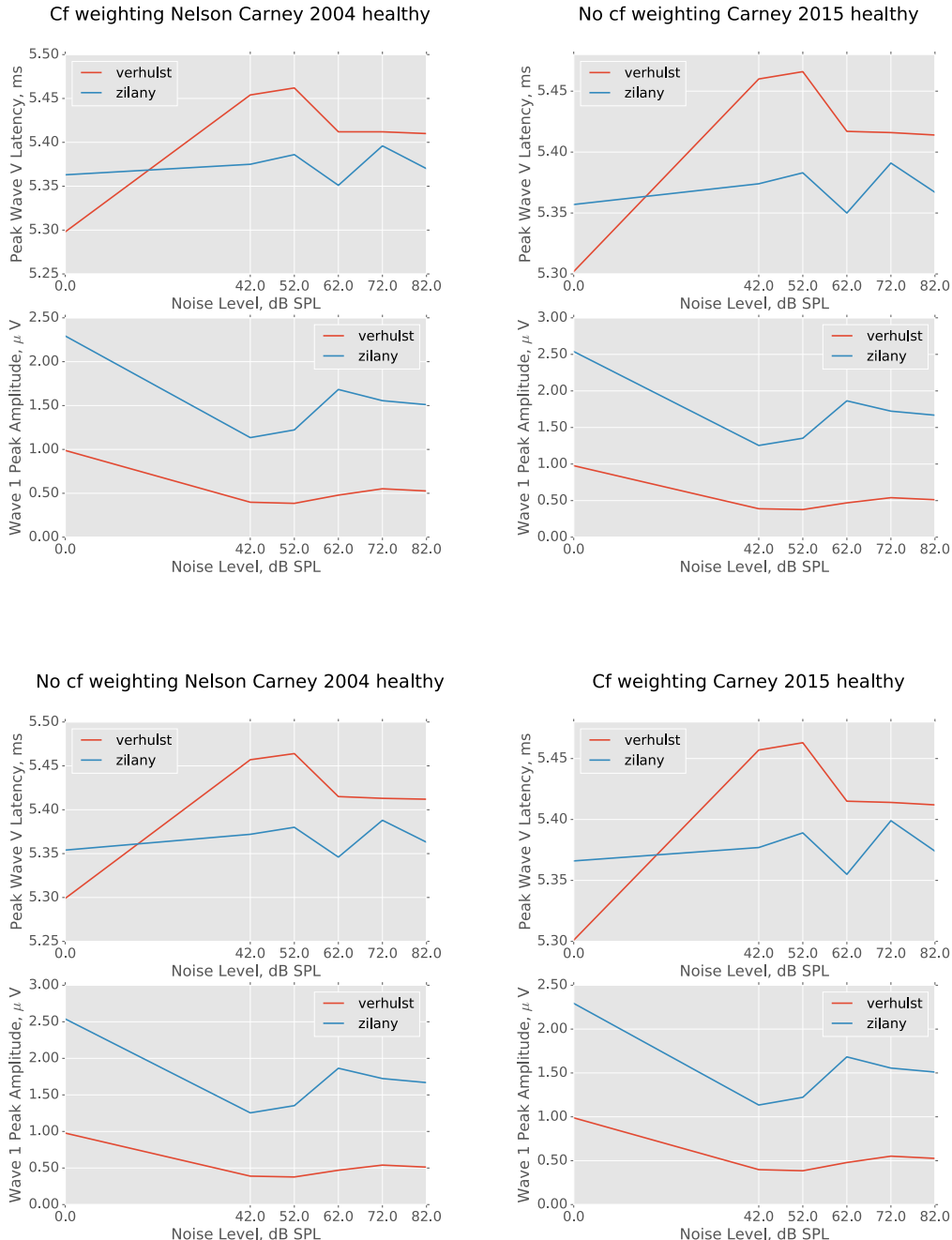


Figure 5.3: Effects of Peripheral Models on Wave I peak amplitude and Wave V peak latency

5.6 Effect of CF weighting

The effects of logically weighing the fiber type distribution along the basilar membrane is given in Figure 5·4. Surprisingly, there was very little relative effect with the Verhulst model to either Wave V latency or Wave I amplitude.

In contrast, the Zilany model showed consistent suppression of Wave V latency and elevation of Wave I amplitudes relative to non-weighted responses.

5.7 Effect of Brainstem Model Choice

The effects of a more complex brainstem model is given in Figure 5·5. No effects are observed for Wave I amplitudes, as Wave I originates at the level of the auditory nerve.

Slight elevations of Wave V latencies are observed with the Zilany periphery.

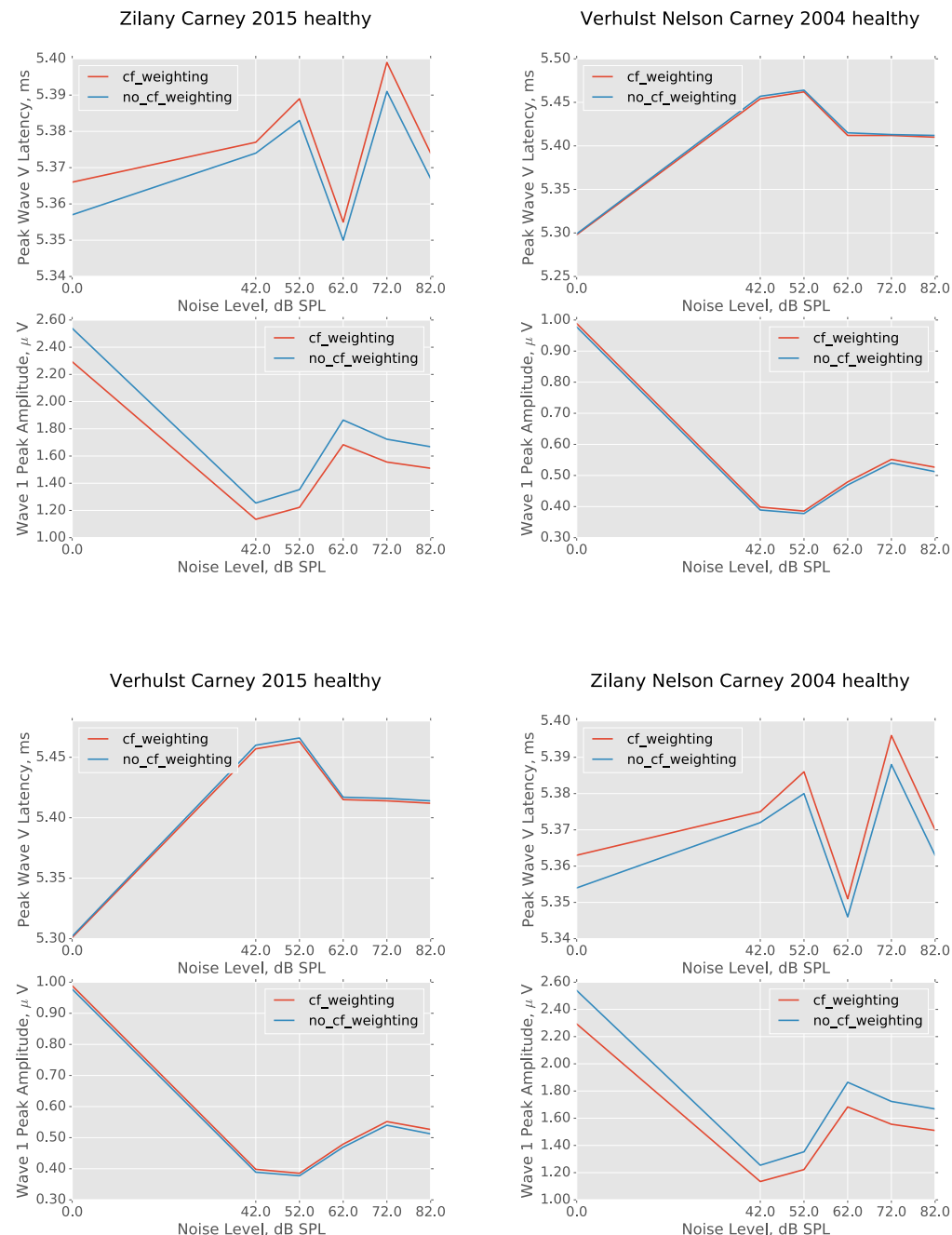


Figure 5.4: Effects of CF Weighting on Wave I peak amplitude and Wave V peak latency

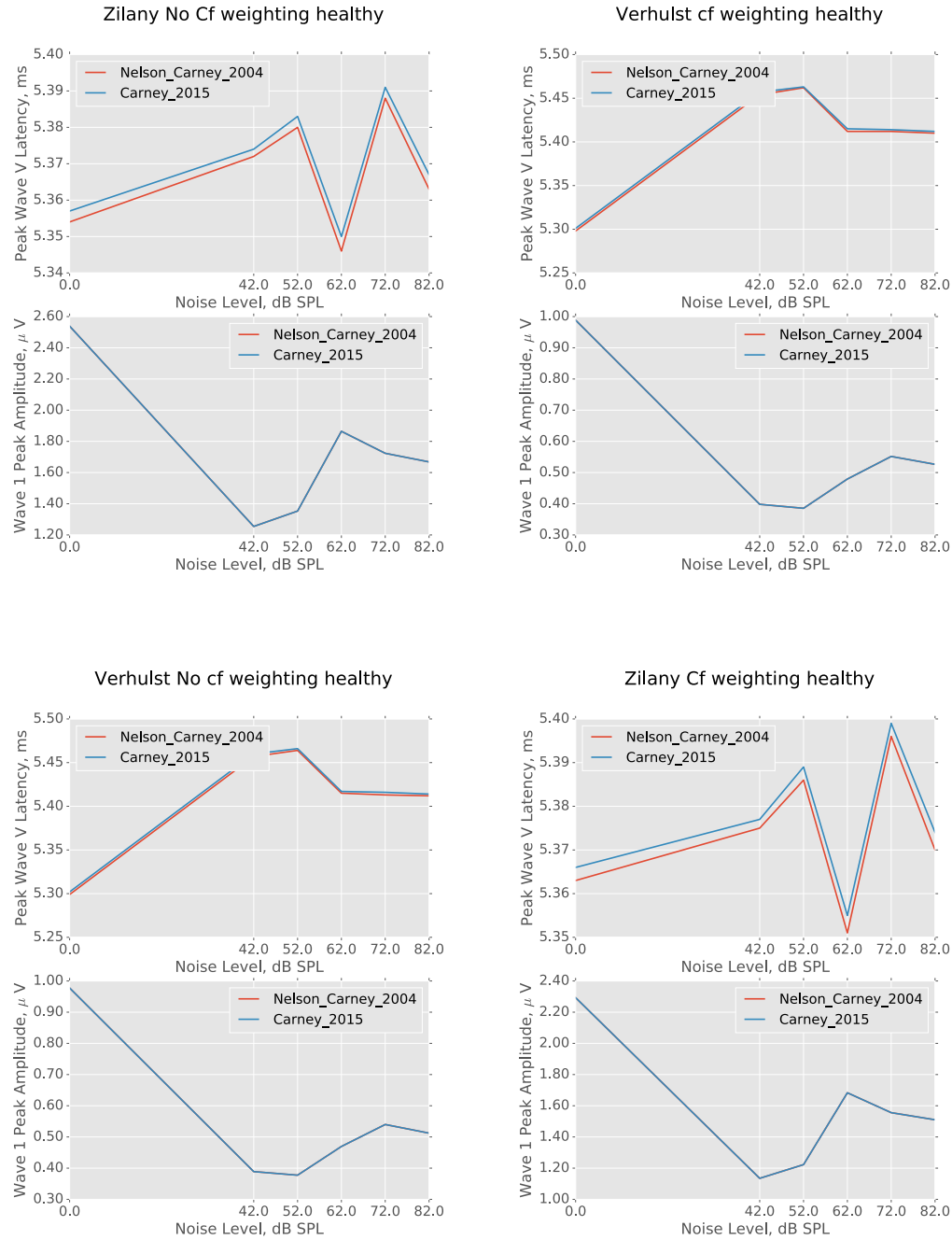


Figure 5.5: Effects of Brainstem Models on Wave V peak latencies. Wave 1 amplitudes arise from the compound action potential of the AN alone, and are unaffected by the brainstem model.

Chapter 6

Discussion

6.1 Chapter Summary

This chapter compares the results obtained in this thesis with the human results obtained by Mehraei et al., 2016, and offers justifications and possible explanations for their similarities and differences.

6.2 Nonlinear Behaviors in the Verhulst Model

During the course of this work, an unexpected phenomenon was observed in the behavior of the Verhulst model in its response to stimuli of long duration. In response to a sustained pure tone stimulus, the model predicts a strong response along the sections of the basilar membrane near the frequency of the pure tone, consistent with intuition. Further, the model predicts small amplitude BM displacement at higher frequencies, correctly reflecting dispersion of energies along the BM. However, at the level of the IHC synapse, the off-frequency firing rate estimates are several times larger than the on-frequency response, and fall outside physiological boundaries. This behavior is not consistent with the BM displacement predictions of the previous stage of the model.

To relate basilar membrane displacement to IHC firing rates, the Verhulst model im-

plements a three-store synaptic diffusion model adapted from Westerman and Smith, 1988 and extends it to have place-dependent initial values of vesicle state. Following Liberman, 1978, the saturated firing rate of a hair cell was also adapted to be place-dependent and used as a reset threshold for the diffusion model parameters. It is possible that in certain situations, this threshold is never reached and thus the firing rate estimate grows disproportionately, leading to the observed large-magnitude response at high frequencies to a low frequency tone.

This behavior would potentially overestimate the off-frequency basal (high frequency) response to a sustained, more apical (low frequency) stimulus. However, some evidence exists (Kiang & Moxon, 1974; Yates, Winter, & Robertson, 1990) that basal responses to apical stimuli can approach threshold in some cases, so a prediction of supra-threshold firing rate at high frequencies to a low frequency tone may not be *a priori* incorrect.

6.3 Consequences of AN Population Response Modeling

To obtain the total contribution of one inner hair cell, and thus one CF, to the population response of the AN, the model scales the responses of a low-, mid-, and high-spontaneous rate modeled fiber by three linear weights, thus reflecting what proportion of spiral ganglia belong to a given category for that IHC. This approach makes two interrelated assumptions.

First, it assumes that the spontaneous behavior of a given fiber is sufficiently similar to that of all others of its spontaneous rate category that it is not necessary to simulate each fiber individually. In the case of the Verhulst model, this assumption is realistic since the model considers spontaneous rates to be fixed per fiber type. However, the Zilany model may be configured so that estimates of spontaneous rate contain

additive white Gaussian noise with a different random seed for every simulation, so the firing statistics of a given fiber may differ both from others of its spontaneous rate class and from itself over sustained periods or repeated simulations.

Second, as a result of the stochasticity of the Zilany model, it would potentially be informative to investigate the loss of individual fibers in a Monte Carlo simulation to address the variance in model responses. This would further complicate simulation and increase the dimensionality of *post-hoc* analysis.

These assumptions make computation of AN responses practical: only three fibers per CF are modeled. Using the default parameters that were used in this work, 3,000 fibers were simulated per model iteration. Simulating each fiber individually with individual stochastic spontaneous rates would incur a tenfold increase in the number of fibers to simulate, suggesting that a full exploration of the parameter space, as was done in this work, would take approximately 90 days to compute.

At the same time, it would more accurately reflect the consequences of cochlear synaptopathy. To the extent that the random noise in a fiber's spontaneous rate is orthogonal to that of any other fiber of the AN, and to the extent that this noise has random phase, any individual fiber will contribute a different amount to the compound action potential of the AN and its loss is not well represented by the current approach.

6.4 Nonlinear Synaptopathic Models

The unexpectedly small effects of modeled synaptopathy on the overall model output may in part be due to the uniformity of the synaptopathic impairment that was simulated. While modeled impairment was specific to fibers of different spontaneous rates, it was applied uniformly over all CFs, as the variability of fiber type distribution

per CF would impair some frequency ranges more than others for a given neuropathic condition.

However, sensorineural hearing loss, particularly age-related hearing loss, is often specific to high frequencies while leaving low frequency bands largely unchanged. Noise-induced or ototoxic hearing loss may have a narrower frequency band, leading to a notched audiogram while leaving other frequencies at normal thresholds, and models of synaptopathy that reflect these more complex losses may have more complex effects on simulation output.

Because the ABR arises from the synchronous activity of entire nerves or brainstem or midbrain areas, a frequency selective perturbation of the output of the AN should produce an effect of greater magnitude than the synaptopathy modeled in this work.

The minimal changes in Wave I peak amplitude are expected. Liberman, Liberman, and Maisor, 2014 and others have demonstrated the robustness of audiometric thresholds in animals with as little as 20% of the original hair cell population intact, so the preservation of the AN compound action potential is consistent even with very severe synaptopathy. Wave I peak amplitudes will also vary with the stimulus.

Chapter 7

Conclusion

7.1 Summary

A model environment that allows the direct differential comparison of two different models of the auditory periphery, the auditory nerve, and two different models of the midbrain and brainstem was created and tested. It incorporates new functionality in the form of a more sophisticated approximation of the population response of the auditory nerve that is aligned with recent anatomical and physiological work.

Further, a tool to robustly explore the summed parameter space of all of the components of the modeling environment was implemented to allow modeling experiments to be reliably designed and run, and produce results that can be analyzed in any language and distributed with confidence.

The utility of the modeling environment was shown in the exploration of the contributions of model parameter effects in the simulation of ABRs. In comparison to human measurements in the same task, the addition of CF-weighted auditory nerve responses more closely matched the experimental results than prior models.

7.2 Future Directions

7.2.1 Modeling of Specific Hearing Loss Types

An important step forward would be the incorporation of more complex synaptopathic degradations. For example, those that result in audiometric threshold shifts, or have frequency-dependent losses as well as SR-dependent losses could provide new insights into the roles of off-frequency listening in a degraded auditory periphery.

Another approach for investigating the role of low-SR fiber loss in HHL could involve the combination of CF weighting of fiber distribution with models of high-frequency hearing loss. At the stimulus levels simulated in this work, frequency tuning along the BM is significantly less sharp than it is at threshold. This broadening of tuning curves has significant implications if fiber loss sufficient to induce HHL occurs preferentially at high frequencies where low-SR fibers are prevalent. In the context of speech in noise, these areas of the cochlea may be thought to be too high frequency to significantly affect speech coding, but at supra-threshold levels, this may not be the case. Consequently, if those same areas synapse with a higher percentage of low-SR, slower-saturating fibers which are preferentially damaged by noise and age, the effects on signal detection in real world environments may be significant.

If high frequency losses are shown to produce degraded representations of speech, this would offer interesting evidence in the possible role of low-SR fibers in nominally off-frequency listening. At sound levels routinely encountered in daily life, frequency tuning curves are quite broad. Potentially, this would allow high frequency areas, which have more low-SR fibers that saturate more slowly, to contribute to AN responses to speech with most energy at lower frequencies. High frequency hearing loss that preferentially damaged low-SR fibers would disrupt that hypothetical mechanism. The modeling environment created for this work could drive prediction and

experimental design to probe this question.

7.2.2 Anatomically Inspired IC Weighting

The proportion of band-pass, band-reject, and low-pass units in Carney et al., 2015 were held fixed throughout this work. However, there is some anatomical evidence to suggest that selectivity in projections from the CN to IC could isolate ascending CN inputs to discrete areas of IC, where the distribution of neural response properties may be nonuniform. This anatomically driven specificity could impose nonuniform latencies on frequency-specific portions of the AN compound action potential, which has the potential to substantially affect Wave V delays.

With the increasingly detailed physiological tools now available, were such inhomogeneities to be characterized, they could be modeled by adapting the IC input weights to more accurately reflect the behavior of the IC to ascending input.

References

- Beebe, N. L., Young, J. W., Mellott, J. G., & Schofield, B. R. (2016, April). Extracellular molecular markers and soma size of inhibitory neurons: evidence for four subtypes of gabaergic cells in the inferior colliculus. *Journal of Neuroscience*, 36(14), 3988–3999. doi:[10.1523/JNEUROSCI.0217-16.2016](https://doi.org/10.1523/JNEUROSCI.0217-16.2016)
- Bharadwaj, H. M., Masud, S., Mehraei, G., Verhulst, S., & Shinn-Cunningham, B. G. (2015, February). Individual differences reveal correlates of hidden hearing deficits. *Journal of Neuroscience*, 35(5), 2161–2172. doi:[10.1523/JNEUROSCI.3915-14.2015](https://doi.org/10.1523/JNEUROSCI.3915-14.2015)
- Bharadwaj, H. M., Verhulst, S., Shaheen, L., Liberman, M. C., & Shinn-Cunningham, B. G. (2014, January). Cochlear neuropathy and the coding of supra-threshold sound. *Frontiers in Systems Neuroscience*, 8, 26. doi:[10.3389/fnsys.2014.00026](https://doi.org/10.3389/fnsys.2014.00026)
- Bourien, J., Tang, Y., Batrez, C., Huet, A., Lenoir, M., Ladrech, S., ... Wang, J. (2014, September). Contribution of auditory nerve fibers to compound action potential of the auditory nerve. *Journal of Neurophysiology*, 112(5), 1025–1039. doi:[10.1152/jn.00738.2013](https://doi.org/10.1152/jn.00738.2013)
- Cant, N. B. & Benson, C. G. (2005, August). An atlas of the inferior colliculus of the gerbil in three dimensions. *Hearing Research*, 206(1-2), 12–27. doi:[10.1016/j.heares.2005.02.014](https://doi.org/10.1016/j.heares.2005.02.014)
- Carney, L. H., Li, T., & McDonough, J. M. (2015, July). Speech coding in the brain: representation of vowel formants by midbrain neurons tuned to sound fluctuations. *eNeuro*, 2(4), 1–12. doi:[10.1523/ENEURO.0004-15.2015](https://doi.org/10.1523/ENEURO.0004-15.2015)
- Cherry, E. C. (1953). Some experiments on the recognition of speech, with one and with two ears. *The Journal of the Acoustical Society of America*, 25(5), 975. doi:[10.1121/1.1907229](https://doi.org/10.1121/1.1907229)
- Covey, E. (2008). Inputs to the inferior colliculus. In *The senses: a comprehensive reference* (1st ed., Chap. 3). San Diego: Academic Press. doi:[10.1016/B978-012370880-9.00053-0](https://doi.org/10.1016/B978-012370880-9.00053-0)
- Durrant, J. D. (2008). Manifestations of cochlear events in the auditory brain-stem response and its clinical applications. In *The senses: a comprehensive reference* (1st ed., Chap. 3, pp. 359–364). San Diego: Academic Press. doi:[10.1016/B978-012370880-9.00031-1](https://doi.org/10.1016/B978-012370880-9.00031-1)
- Fernandez, K. a., Jeffers, P. W. C., Lall, K., Liberman, M. C., & Kujawa, S. G. (2015). Aging after noise exposure: acceleration of cochlear synaptopathy in “recovered”

- ears. *Journal of Neuroscience*, 35(19), 7509–7520. doi:10.1523/JNEUROSCI.5138-14.2015
- Furman, A. C., Kujawa, S. G., & Liberman, M. C. (2013, August). Noise-induced cochlear neuropathy is selective for fibers with low spontaneous rates. *Journal of Neurophysiology*, 110(3), 577–86. doi:10.1152/jn.00164.2013
- Kiang, N. Y. & Moxon, E. C. (1974, March). Tails of tuning curves of auditory-nerve fibers. *The Journal of the Acoustical Society of America*, 55(3), 620–30. doi:10.5056/jnm15129
- Kujawa, S. G. & Liberman, M. C. (2009, November). Adding insult to injury: cochlear nerve degeneration after “temporary” noise-induced hearing loss. *Journal of Neuroscience*, 29(45), 14077–85. doi:10.1523/JNEUROSCI.2845-09.2009
- Liberman, M. C. (1978, February). Auditory-nerve response from cats raised in a low-noise chamber. *The Journal of the Acoustical Society of America*, 63(2), 442–55. Retrieved from <http://www.ncbi.nlm.nih.gov/pubmed/670542>
- Liberman, M. C., Liberman, L. D., & Maisor, S. F. (2014, March). Efferent feedback slows cochlear aging. *Journal of Neuroscience*, 34(13), 4599–4607. doi:10.1523/JNEUROSCI.4923-13.2014
- Liberman, M. C. (1993, January). Central projections of auditory nerve fibers of differing spontaneous rate, ii: posteroverentral and dorsal cochlear nuclei. *The Journal of Comparative Neurology*, 327(1), 17–36. doi:10.1002/cne.903270103
- Meddis, R. & Lopez-Poveda, E. A. (2010). *Computational models of the auditory system*. Springer Handbook of Auditory Research. Boston, MA: Springer US. doi:10.1007/978-1-4419-5934-8
- Mehraei, G., Hickox, A. E., Bharadwaj, H. M., Goldberg, H., Verhulst, S., Liberman, M. C., & Shinn-Cunningham, B. G. (2016, March). Auditory brainstem response latency in noise as a marker of cochlear synaptopathy. *Journal of Neuroscience*, 36(13), 3755–3764. doi:10.1523/JNEUROSCI.4460-15.2016
- Mehraei, G. (2015). *Auditory brainstem response latency in noise as a marker of cochlear synaptopathy* (Doctoral dissertation, Massachusetts Institute of Technology).
- Mehraei, G., Gallardo, A. P., Epp, B., Shinn-Cunningham, B., & Dau, T. (2015, April). Individual differences in auditory brainstem response wave-v latency in forward masking: a measure of auditory neuropathy? *Journal of the Acoustical Society of America*, 137(4), 2207–2207. doi:10.1121/1.4920035
- Meyer, R. & Obermayer, K. (2016). Pypet: the python parameter exploration toolkit.
- Moore, D. R. & Kitzes, L. M. (1985, October). Projections from the cochlear nucleus to the inferior colliculus in normal and neonatally cochlea-ablated gerbils. *The Journal of Comparative Neurology*, 240(2), 180–195. doi:10.1002/cne.902400208
- Nelson, P. C. & Carney, L. H. (2004). A phenomenological model of peripheral and central neural responses to amplitude-modulated tones. *The Journal of the Acoustical Society of America*, 116(4), 2173. doi:10.1121/1.1784442

- Rudnicki, M. & Hemmert, W. (2014). Cochlea: inner ear models in python. München, Germany. Retrieved from <https://github.com/mrkrd/cochlea>
- Ryugo, D. (2008, June). Projections of low spontaneous rate, high threshold auditory nerve fibers to the small cell cap of the cochlear nucleus in cats. *Neuroscience*, 154(1), 114–126. doi:[10.1016/j.neuroscience.2007.10.052](https://doi.org/10.1016/j.neuroscience.2007.10.052)
- Schaette, R. & McAlpine, D. (2011, September). Tinnitus with a normal audiogram: physiological evidence for hidden hearing loss and computational model. *Journal of Neuroscience*, 31(38), 13452–7. doi:[10.1523/JNEUROSCI.2156-11.2011](https://doi.org/10.1523/JNEUROSCI.2156-11.2011)
- Sergeyenko, Y., Lall, K., Liberman, M. C., & Kujawa, S. G. (2013, August). Age-related cochlear synaptopathy: an early-onset contributor to auditory functional decline. *Journal of Neuroscience*, 33(34), 13686–13694. doi:[10.1523/JNEUROSCI.1783-13.2013](https://doi.org/10.1523/JNEUROSCI.1783-13.2013)
- Temchin, A. N., Rich, N. C., & Ruggero, M. A. (2008, August). Threshold tuning curves of chinchilla auditory nerve fibers. ii. dependence on spontaneous activity and relation to cochlear nonlinearity. *Journal of Neurophysiology*, 100(5), 2899–2906. doi:[10.1152/jn.90639.2008](https://doi.org/10.1152/jn.90639.2008)
- Temchin, A. N. & Ruggero, M. A. (2014, August). Spatial irregularities of sensitivity along the organ of corti of the cochlea. *Journal of Neuroscience*, 34(34), 11349–54. doi:[10.1523/JNEUROSCI.2558-13.2014](https://doi.org/10.1523/JNEUROSCI.2558-13.2014)
- Verhulst, S., Bharadwaj, H. M., Mehraei, G., Shera, C. A., & Shinn-Cunningham, B. G. (2015, September). Functional modeling of the human auditory brainstem response to broadband stimulations. *The Journal of the Acoustical Society of America*, 138(3), 1637–1659. doi:[10.1121/1.4928305](https://doi.org/10.1121/1.4928305)
- Voysey, G. E. (2016). Corti, a flexible modeling environment for evaluating subcortical auditory systems. Boston, MA. doi:[10.5281/zenodo.57111](https://doi.org/10.5281/zenodo.57111)
- Westerman, L. A. & Smith, R. L. (1988, June). A diffusion model of the transient response of the cochlear inner hair cell synapse. *The Journal of the Acoustical Society of America*, 83(6), 2266–76. Retrieved from <http://www.ncbi.nlm.nih.gov/pubmed/3411018>
- Yates, G. K., Winter, I. M., & Robertson, D. (1990, May). Basilar membrane nonlinearity determines auditory nerve rate-intensity functions and cochlear dynamic range. *Hearing Research*, 45(3), 203–219. doi:[10.1016/0378-5955\(90\)90121-5](https://doi.org/10.1016/0378-5955(90)90121-5)
- Zilany, M. S. A. & Bruce, I. C. (2006). Modeling auditory-nerve responses for high sound pressure levels in the normal and impaired auditory periphery. *The Journal of the Acoustical Society of America*, 120(3), 1446. doi:[10.1121/1.2225512](https://doi.org/10.1121/1.2225512)
- Zilany, M. S. A. & Bruce, I. C. (2007, May). Predictions of speech intelligibility with a model of the normal and impaired auditory-periphery. In *2007 3rd international ieee/embs conference on neural engineering* (pp. 481–485). IEEE. doi:[10.1109/CNE.2007.369714](https://doi.org/10.1109/CNE.2007.369714)
- Zilany, M. S. A., Bruce, I. C., & Carney, L. H. (2014, January). Updated parameters and expanded simulation options for a model of the auditory periphery. *The*

Journal of the Acoustical Society of America, 135(1), 283–286. doi:[10.1121/1.4837815](https://doi.org/10.1121/1.4837815)

Zilany, M. S. A., Bruce, I. C., Nelson, P. C., & Carney, L. H. (2009). A phenomenological model of the synapse between the inner hair cell and auditory nerve: long-term adaptation with power-law dynamics. *The Journal of the Acoustical Society of America*, 126(5), 2390. doi:[10.1121/1.3238250](https://doi.org/10.1121/1.3238250)